Aβ42 induces selective degeneration in hippocampal cells of aged monkeys

Laiqiang Chen[1,2]#, Jiawei Zhang[2]#, Zhifu Wang[2,3]#, Yu-Heng Ma[2,3], Yingqi Lin[2,3], Xichen Song[2,3], Xiaopeng Luo[2,3], Kecheng Chen[2,3], Lu Wang[4], Hao Xu[4], Shihua Li[2,3], Sen Yan[2,3], Xiangyu Wang[1], Jun Wen[1]*, Weili Yang[2,3]*, Bang Li[2,5]*, Xiao-Jiang Li[2,3,6]*

[1]Department of Neurosurgery, First Affiliated Hospital of Jinan University, Guangzhou 510630, China

[2]Guangdong Provincial Key Laboratory of Non-human Primate Research, GHM Institute of CNS Regeneration, Jinan University, Guangzhou 510632, China

[3]State Key Laboratory of Bioactive Molecules and Druggability Assessment, Guangzhou 510632, China

[4]Center of Cyclotron and PET Radiopharmaceuticals, Department of Nuclear Medicine and PET/CT-MRI Center, the First Affiliated Hospital of Jinan University, Guangzhou 510630, China

[5]College of A&F Engineering and Planning, Tongren University, Tongren, Guizhou 554300, China

[6]Lingang Laboratory, Shanghai 201306, China

#The first three authors contributed equally to the work

*Corresponding authors

Lead contact: Xiao-Jiang Li,
Email: xjli33@jnu.edu.cn,
GHM Institute of CNS Regeneration,
Jinan University, Guangzhou, 510632, China

Science Press
ZR Zoological Research

ABSTRACT

The hippocampus is one of the earliest and most severely affected brain regions in Alzheimer's disease (AD) and is critical for memory formation. However, the precise mechanisms through which AD disrupts hippocampal neurons remain poorly understood. To investigate the effects of Aβ42 in a model closer to humans, we performed stereotaxic injections of an AAV9 vector encoding human Aβ42 into the hippocampus of young (7-year-old) and aged (>20-year-old) cynomolgus monkeys. We found that AAV9-mediated Aβ42 expression induced more severe neuropathology, reduced daytime activity, and increased sleep disturbances in aged monkeys compared to young controls. snRNA-seq revealed an age-dependent reduction in disease-associated microglia (DAM II) in the aged hippocampus. Furthermore, we identified a specific subtype of hippocampal pyramidal neuron (*TRPS1*$^{+}$*RELN*$^{+}$) that is selectively vulnerable to Aβ42 toxicity in aged monkeys. Our findings indicate that Aβ42 toxicity is exacerbated in the aged primate hippocampus due to a combination of microglial decline and the selective vulnerability of a distinct neuronal subtype (*TRPS1*$^{+}$*RELN*$^{+}$ PCs). This identified subtype represents a new potential therapeutic target for treating hippocampal dysfunction in AD.

Keywords: Alzheimer's disease; Amyloid pathology; Non-human primate; Aging; Neurodegeneration

INTRODUCTION

In Alzheimer's disease (AD), the accumulation of two key proteins, amyloid-beta (Aβ) and tau, is central to the disease process. The prevailing hypothesis suggests that the accumulation of Aβ may occur earlier in the disease process, preceding the aggregation and spread of tau pathology (Goedert & Spillantini, 2006; Long et al., 2019; Chang et al., 2021; Zhang et al., 2025). Aβ accumulation is thought to initiate a cascade of events including the spread of neurofibrillary tangle (NFT) tau pathology, ultimately resulting in neurodegeneration and cognitive decline (Long et al., 2019). Supporting this theory, mutations in genes such as the amyloid precursor protein (APP) and enzymes that generate Aβ (including presenilin 1 (PSEN1) and presenilin 2 (PSEN2) have been identified in familial early-onset AD cases (Tanzi & Bertram, 2005; Hardy et al., 2017). Mutations in these genes can lead to the overproduction of Aβ or the generation of more aggregation-prone forms of Aβ (Levy et al., 1990; Goate et al., 1991). Also, duplication of the APP locus results in accumulation of amyloid-beta peptides and causes early-onset AD in humans

(Rovelet-Lecrux et al., 2006). Transgenic animal models expressing mutant forms of *APP* or *PSEN* genes have been widely used to investigate AD pathogenesis (Jankowsky & Zheng 2017; Kshirsagar et al., 2022; Pan et al., 2024), whereas BACE1, an enzyme that is essential for the generation of Aβ42, knockout mice do not produce Aβ42 and are free from Alzheimer's associated pathologies (Cole & Vassar, 2007). Furthermore, recent studies show the promising effects that monoclonal antibodies against Aβ can remarkably eliminate Aβ plaques in the brains of AD patients, with encouraging, though modest, effects on improving cognitive functions (Jucker & Walker, 2023; Shi et al., 2024; Rafii & Aisen, 2025).

Although Aβ accumulation is often considered an early event in AD and genetic mutations in APP cause early-onset familial AD, the mechanism underlying Aβ-mediated neurodegeneration in AD remains to be investigated. Many previous studies have investigated the pathogenic role of Aβ in a variety of animal models and provide important insights. Of these animal models, non-human primates are most similar to humans in aging, brain anatomy, and physiology and have also been used to establish AD animal models (Wang et al., 2024; Pan et al., 2024). The advantage of using non-human primates is to identify early neuropathological phenotypes of AD, which are difficult to uncover from post-mortem brain tissues of AD patients who often undergo disease progression for decades.

Hippocampal function, which is essential for memory and cognition, is profoundly impaired in AD. While studies using rodent models and postmortem human AD brains have provided valuable insights, the impact of AD on hippocampal neuronal degeneration remains poorly understood, largely due to the difficulty of studying early disease stages in humans. In this study, we used an AAV approach to express Aβ42 in the hippocampus of young and aged cynomolgus monkeys. We found that Aβ42 forms more abundant aggregates and triggers more severe neuropathology in aged monkeys (over 20 years old). Furthermore, we identified a specific subtype of hippocampal neurons that is particularly susceptible to Aβ42 toxicity in the aged brain. This research provides new insights into how Aβ42 causes hippocampal dysfunction in AD and proposes a novel target for improving hippocampal function and mitigating AD phenotypes.

MATERIALS AND METHODS

Monkeys

A total of 16 cynomolgus (*Macaca fascicularis*) monkeys were used for brain stereotaxic injection in the study (Table 1). The monkeys were individually housed at Guangdong Landao

Biotechnology Co. Ltd, Guangzhou, which is an Association for Assessment and Accreditation of Laboratory Animal Care (AAALAC) accredited facility. Water, food, temperature, and humidity of the home cages were closely monitored. The health conditions of the monkeys were examined daily by certified veterinarians. All animal procedures were approved by the Institutional Animal Care and Use Committee at Guangdong Landao Biotechnology Co. Ltd, Guangzhou. This study was conducted in strict compliance with the ‘‘Guide for the Care and Use of Laboratory Animals of the Institute of Laboratory Animal Science (est. 2006)’’ and ‘‘The use of non-human primates in research of the Institute of Laboratory Animal Science (est. 2006)’’ to ensure the safety of personnel and animal welfare.

Animal information is provided in Table 1.

AAV stereotaxic brain injection into adult monkeys

Human Aβ42 (amyloid-beta 42) was linked to the C-terminus of BRI (British amyloid precursor protein) as described previously (Lewis et al., 2001; McGowan et al., 2005; Kim et al., 2013). We used AAV9 to express BRI (control) and BRI-Aβ42. Viral vectors were packaged to generate purified AAV9 viruses by Guangzhou Paizhen Biotechnology Co. Ltd, China. The genomic titer of viruses (vg) (approximately 1×10^{13} vg/ml) of the purified viruses, which were used for injection, was determined by a PCR method.

Viral injection into the monkey hippocampus was performed using the method described in our previous studies (Tu et al., 2023). The monkey brain regions were located by MRI before injection and the animals were deprived of food and water the night before surgery. Each monkey was anesthetized by intraperitoneal injection of 0.3–0.5 mL of atropine, followed by 10–12 mg of ketamine and 15–20 mg of pelltobarbitalum natricum per kg body weight. The monkeys were then stabilized on a stereotaxic instrument (David Kopf Instruments, USA). A volume of 45 μL (1×10^{13} vg/mL) of viruses was injected into one side of the monkey hippocampus. The left side of the brain region was injected with AAV9-BRI-Aβ42 and the right side was injected with control AAV9-BRI. Three or 12 months after injection, the monkeys were euthanized by deep anesthesia with intraperitoneal injection of 0.3–0.5 mL of atropine, followed by 10–12 mg of ketamine and 15–20 mg of pelltobarbitalum natricum per kg body weight. The brain tissues of the monkeys were then isolated for immunohistochemical, western blotting, and scRNA analyses.

Antibodies and reagents

The following antibodies were used in the study: TRPS1 (CST, 17936, IF:1:100, USA); Flag (Sigma F1804, WB:1:1000, USA); NeuN (Abcam, Ab177487, WB:1:1000, England); NeuN

(Millipore ABN90, IF 1:2000, USA); GFAP (Abcam Ab7260, WB 1:1000, England); GFAP (Themofisher G3893, IF 1:1000, USA); Aβ42 (Abcam Ab240360, WB :1:5000, England); IBA1 (Wako 018-28523, WB 1:3000, Japan); p-TAU (Themofisher MN1020, IF :1:300, USA); Vinculin (Millipore MAB3574, WB :1:1000, USA); PSD95 (Abcam Ab238135, WB :1:5000, IF: 1:1000, England); Snap25 (Abcam Ab41455, WB:1:5000, England).

Western blot analysis

For western blot analysis, monkey brain tissues were lysed in ice-cold RIPA buffer (50 mM Tris, pH 8.0, 150 mM NaCl, 1 mM EDTA pH 8.0, 1 mM EGTA pH 8.0, 0.1% SDS, 0.5% DOC, 50 mM NaF and 1% Triton X-100) containing Halt protease inhibitor cocktail (Thermo Scientific, USA) and PMSF. The lysates were incubated on ice for 30 min, sonicated, and centrifuged at maximum speed for 10 min. Equal amounts of proteins from the supernatants, determined by BCA assay, were resolved by SDS-PAGE and subjected to western blot analysis with appropriate primary antibodies. Independent western blot experiments were performed at least three times, and representative results are presented in figures. Acquired images were subjected to densitometric quantification using ImageJ software.

Immunofluorescent staining

For immunofluorescent staining, monkey brain tissues were sliced into slabs approximately a centimeter thick, then they were post-fixed in 4% PFA (paraformaldehyde) in 0.01 mol/L PBS at 4°C for 5 days. After that, they were cryopreserved in 15% sucrose in 0.01 mol/L PBS at 4°C for 3 days. When the tissues sank to the bottom, they were transferred into 30% sucrose at 4°C for 10 days until the brain tissue completely sank to the bottom of the tube. 30 μm thick coronal sections were cut using a cryotome, incubated first in a blocking solution (2% normal goat serum, 3% BSA, 0.3% Triton X-100 in PBS), then with primary antibodies against relevant proteins for 18 h at 4 °C, and next with secondary antibodies and Hoechst diluted in 0.3% Triton X-100 in PBS. To remove the interference caused by lipofuscin, slices were incubated with 0.3% Sudan black (in 70% ethanol diluted by 1×PBS) for 3 min, and then washed with 0.3% Triton X-100 in PBS. Double immunofluorescence staining was analyzed using a confocal imaging system (Olympus FV3000 Microscope). The brain region was cut into 25 μm sections. Four to five images were captured per section. The number of cells labeled with specific antibodies and Aβ42 aggregates per image was counted. The data were presented as mean±SEM for statistical analysis.

MRI image acquisition and PET/CT imaging

MRI scanning was conducted as described in our previous work (Li et al., 2023). Briefly, the monkeys were anesthetized with ketamine (10 mg/kg, i.m.) and placed into the scanner in the prone position for a T1-weighted 3-dimensional MR scan. The scans were performed on a 3.0 T MR machine (Siemens MAGNETOM 3T Prisma) using a custom-designed 8-channel radio-frequency surface head coil at Guangdong Laboratory Animals Monitoring Institute. The whole brain images were acquired with a 3D Bravo T1 sequence (TR = 5000 ms, TE = 2.31 ms, slice thickness = 0.3 mm, matrix size = 120×120, FOV = 12×12 cm), a T2 SPACE dark sequence (TR = 3500 ms, TE = 178 ms, slice thickness = 0.3 mm, matrix size = 120×120, FOV = 12×12 cm), and a T2 FLAIR sequence (TR = 6500 ms, TE = 184 ms, slice thickness = 0.5 mm, matrix size = 120×120, FOV = 12×12 cm).

PET-CT scanning was conducted at the PET/CT-MRI Center, the First Affiliated Hospital of Jinan University (JNUH) as described in our previous work (Tu et al., 2019; Han et al., 2024). The PET tracer, [^{11}C]PIB (Pittsburgh Compound B), which is used to visualize and quantify beta-amyloid plaques in the human brain for the assessment of AD (Ruan & Sun 2023; Lopresti et al., 2025), was radiolabeled in the Center of Cyclotron and PET Radiopharmaceuticals (CCPR) at JNUH. Briefly, animals were deprived of food for 12 h before tracer injection. The mean dose of [^{11}C]PIB administered was 0.5 mCi/kg body weight (18.5 MBq/kg). The animal was placed in the imaging chamber and anesthetized with a 2.0% isoflurane/oxygen gas mixture throughout the imaging experiment. Body temperature was maintained at 37°C and monitored during anesthesia. Head position was fixed with a stereotactic frame. A CT scan was performed first, followed by a 10-minute static positron emission data collection at 60 min post-injection. CT data were acquired with breath-hold at 140 kV, 230 mA modulated using the GE AutomA technique (GE Medical System, USA) with a noise index of 30, slice thickness of 3.75 mm, slice interval of 3.27 mm, matrix size of 256 × 256 and a scan FOV of 70 cm. Data analysis was performed using PMOD® version 4.1 (Pmod Technologies LLC, Switzerland). The uptake of PET tracers in the occipital cortex was used as a reference for SUVr analysis as previously described. The co-registration of the PET image to the individual MR image, which was transformed into a brain template MR image, was carried out following published protocols (Tu et al., 2019).

Behavioral Analysis

The delayed response (DR) task was conducted using the Wisconsin General Test Apparatus (WGTA) (Herndon et al., 1997; Tu et al., 2023), where a monkey was positioned in its home cage facing a tray equipped with two food wells, each covered by identical hinged lids. In each trial, the experimenter placed food in one of the wells in full view of the monkey, covered the well, and then

lowered an opaque screen to obstruct the monkey's view of the tray. Following a predetermined delay period, termed the memory retention interval, the screen was raised, allowing the monkey to select the baited well by recalling its location from working memory. Across 30 daily trials, the food reward was randomly assigned to one of the two wells. The initial memory retention interval for each monkey was set at 3 seconds. This interval was incrementally extended using a stepwise protocol when the monkey achieved at least 26 correct responses out of 30 trials per day for three consecutive days, indicating mastery of the interval. If a monkey failed to master a given interval within one week, the DR task was concluded, and the longest interval successfully mastered was recorded for analysis. The task protocol was consistently applied to both control and Aβ-overexpressing groups, both pre- and postoperatively. Completion of the task typically required approximately four weeks for most monkeys.

Reversal learning was conducted utilizing the Wisconsin General Test Apparatus (WGTA) (Lai et al., 1995; Makori et al., 2013). A stimulus tray with two identical, equally spaced wells, each covered by one of two distinct objects, was concealed from the monkey by an opaque screen during trial preparation. Rewards, consisting of raisins, cereal, or uniformly sized fruit pieces, were placed in the designated well per the task protocol, and the monkey's response was observed through a one-way vision panel after raising the screen. A non-correction procedure was employed, terminating trials without reward upon incorrect responses. In the initial learning phase, one object was randomly designated as the positive (baited) stimulus, with object positions varied across trials using a pseudorandom sequence to ensure spatial location was not a relevant cue. Monkeys obtained rewards by displacing the object covering the baited well, with a 20-second intertrial interval (ITI) during which the screen was lowered and the designated object baited for the next trial. Thirty trials were conducted daily until the monkey achieved ≥90% correct responses (27/30 trials) over 30 consecutive trials. Subsequently, a single reversal was initiated the following day, with the previously unrewarded object becoming the baited stimulus, continuing with 30 trials per day until ≥90% correct responses (18/20 trials) were achieved in the first 20 trials of a session.

Activity Level Assessment was conducted as described in previous work (Chen et al., 2017; Noser et al., 2013). The physical activity of free-moving monkeys was monitored using Actical Physical Activity Monitors (Respironics, Pennsylvania, USA). The monitors employ a single omni-directional accelerometer that detects motion in all directions. The system integrates both the amplitude and frequency of the detected motion, generating a corresponding electrical current whose magnitude is proportional to the intensity of the motion. Activity data were stored as activity counts, which were later used for analysis. For the study, five Aβ42-injected monkeys and five age-matched wild-type (WT) controls were monitored over a period of 6 days. Prior to data

collection, each monkey's unique ID, body weight, and length were input into the Actical software (v.3.1.0). The device was securely mounted at the same neck position on each monkey using a soft belt, ensuring consistency in data collection. Data were recorded with a sampling rate of 32 Hz and in 1-second epochs to capture high-resolution activity patterns. Data were downloaded using the Actireader, which connected to a PC via an RS-232 serial cable. Communication between the Actireader and Actical monitors was facilitated via a short-range telemetric link. This setup allowed for continuous monitoring of the monkeys' activity levels throughout the study period.

Sleep Pattern Assessment was conducted as previously described (Chen et al., 2017; Noser et al., 2003). The sleep behaviors of 10 cynomolgus monkeys, including 5 Aβ42-injected mutants and 5 age-matched wild-type (WT) controls, were continuously video-recorded over 6 consecutive nights, from 1900h to 0700h. The recording system consisted of 10 infrared video cameras, each positioned to capture a single cage, ensuring full visibility of the animals' behavior. A hard disk video recorder was used to store the footage. Three independent raters, blinded to the experimental conditions, scored the video recordings. The monkeys' sleep behaviors were categorized into two states: awake and transitional sleep. Behaviors were scored in 1-minute epochs. States lasting less than 30 seconds were excluded from the analysis, while those lasting between 30 and 59 seconds were rounded to 1 minute. A monkey was classified as awake if it exhibited locomotion or more than three body or limb movements within a 1-minute period while sitting or lying down. Transitional sleep was defined as a state in which 1 or 2 body or limb movements occurred within 1 minute, either while the monkey was sitting or lying immobile. Sleep duration was quantified as the total time spent in transitional sleep. Sleep fragmentation was assessed by counting the number of wake bouts lasting 1 minute or longer during the night.

Single-nucleus RNA sequencing

The left and right hippocampus tissues of the euthanized monkeys were dissected and collected separately. To collect the whole hippocampal region as completely as possible, each single hippocampus was flattened to capture the entire superficial layer and placed into a tube. The collected tissues were kept at 4°C and sent to Dynamic Biosystems Inc. (Suzhou, China) to isolate the cellular nuclei for performing the single-nucleus sequencing with the Well-Paired-Seq platform. The raw sequencing reads were aligned to the Ensembl reference (Macaca_fascicularis_5.0) and counted using the DynamicEX software (v.1.0.3). A Seurat (v.3.1.3) object of each sample was constructed from the decontaminated matrix, and cells with fewer than 200 genes or mitochondrial ratio greater than 5% were discarded (Butler et al., 2018). Doublet detection was performed with

DoubletFinder (v.2.0.2) (McGinnis et al., 2019). The samples were integrated and the batch effects were adjusted with Harmony (v.0.1) (Korsunsky et al., 2019). After sample integration and clustering as mentioned below, clusters lacking specific marker genes and with relatively low gene content and high mitochondrial ratio were also discarded. After data integration and scaling, principal component analysis was applied with the "RunPCA" function, and appropriate principal components were selected for the subsequent analyses. Dimensionality was reduced with the "RunUMAP" function. "FindNeighbors" and "FindClusters" functions were applied to perform clustering. Marker genes for each cluster were identified by the "FindAllMarkers" function with the cutoff of adjusted *P*-values<0.05 and $|\log_2(\text{foldchange})|>0.25$. The marker genes used to identify the clusters were described above.

Quantification and statistical analysis

We used samples from multiple animals (Table 1) and freshly frozen brain tissues from WT monkeys that were collected in our previous studies. When analyzing western blots, at least three independent experiments were conducted, and densitometric results were quantified. Immunofluorescent parameters were measured in 4-5 random fields per brain section, with the sample size (n) representing the number of sections analyzed. The results are based on sections obtained from a minimum of two animals. For Western blot quantification, the intensity ratios of target proteins to loading controls were calculated from at least three biological replicates. Statistical significance was assessed using the two-tailed Student's *t*-test or paired *t*-test for comparing two groups, and a *P*-value less than 0.05 was considered significant. Comparisons involving three or more groups were analyzed using *one-way ANOVA*, with post hoc pairwise comparisons between groups adjusted by the Bonferroni test. Data presented in figures represent the mean±SEM. Calculations were performed using GraphPad Prism software (v.9.5.1).

RESULTS

Neuropathology in the aged monkey brain cortex following Aβ42 expression

Using Aβ (amyloid-beta) proteins isolated from the brains of AD patients or synthetic amyloid-beta oligomers for injecting them into monkey brains has been utilized as a research model to investigate in vivo Aβ42 toxicity (Beckman et al., 2019; Gary et al., 2019; Lam et al., 2021; Yue et al., 2021). Since there are variations in the structural viability and stability of these

materials in animal brains, we opted to use AAV to express Aβ42 due to its superior consistency and long-term expression capabilities in monkey brains. Aβ42 was linked with BRI (British amyloid precursor protein) for viral expression in animal brains because this fusion enhances the solubility of Aβ42 and improves its processing and release within the brain (Lewis et al., 2001; McGowan et al., 2005; Kim et al., 2013).

We generated a DNA construct to express Aβ42 fused to BRI, with an N-terminal Flag epitope tag, under the control of the UBC promoter. As a control, we used a construct expressing only BRI. Both constructs were packaged into AAV9 for infection of cultured HEK293 cells and stereotaxic injection into monkey brains (Figure 1A). Western blot analysis confirmed the expression of BRI-Aβ42, which migrated slightly larger than BRI alone when probed with an anti-Flag antibody. Notably, only the BRI-Aβ42 fusion protein was detected by the anti-Aβ antibody (ab240360) (Figure 1B). Immunostaining of transfected HEK293 cells further demonstrated that Aβ42 expression was specifically detected by the anti-Aβ antibody (Figure 1C). We then performed stereotaxic injections of AAV9-BRI-Aβ42 (referred to as AAV-Aβ42) into the prefrontal cortex (PFC) of aged monkeys (~25-year-old) (Figure 1D). As a control, the contralateral side of the prefrontal cortex was injected with AAV9-BRI (referred to as AAV-control). Immunostaining of the Aβ42-injected cortex using the anti-Aβ42 antibody confirmed robust Aβ42 expression (Figure 1E). At higher magnification, we observed clear and increased Aβ plaque formation (P>0.05) in the AAV-Aβ42 virus injected PFC tissues (n=3) compared to the control group (n=3) (Figure 1F), resembling plaques found in transgenic BRI-Aβ mouse brains, where furin-mediated proteolytic cleavage releases Aβ from the fusion protein (Lewis et al., 2001; McGowan et al., 2005). Western blot analysis with the anti-Aβ42 antibody detected Aβ42 product in the injected brain tissues, which was absent in the control (arrow, Figure 1G).

Unlike transgenic BRI-Aβ42 mice, which show no neuronal loss (McGowan et al., 2005), Aβ42 expression in the monkey PFC resulted in reduced neuronal density in layer III and layer V regions compared to the control group (n=3 for each group) (Figure 2A). To confirm that the brain region with fewer neurons also exhibited Aβ42 plaques, we performed double immunostaining with NeuN and GFAP antibodies. The results revealed that Aβ42 plaques were associated with fewer NeuN-positive cells and increased GFAP signal (Figure 2B), a marker of reactive astrocytes that is upregulated during neurodegeneration. Quantification of NeuN-positive (n = 8 slices for each group) and GFAP-positive cells (n = 18 slices for each group) in Aβ42-expressing regions further demonstrated a significant decrease in NeuN and an increase in GFAP compared to control-injected areas (Figure 2C). Together, these results indicate that AAV-mediated BRI-Aβ42

expression in the monkey brain induces Aβ plaque deposition and primate-dependent neuronal loss.

Age-dependent neuropathology mediated by Aβ42 in the monkey hippocampus

Given that AD is characterized by age-dependent memory impairment, we proceeded to use AAV stereotaxic injection into the hippocampus of young (~7 years) and aged (~26 years) monkeys to explore the effects of Aβ42 on this brain region. We unilaterally injected AAV-Control (10 μl, $1x10^{13}$ vg/ml) into the left side and AAV-Aβ42 (10 μl, $1x10^{13}$ vg/ml) into the right side of the hippocampus in the same monkey to thoroughly assess Aβ42 toxicity (Figure 3A). Aβ42 immunostaining revealed no detectable plaque signals in the hippocampus of the young monkey that received the control injection whereas the aged monkey displayed a few Aβ42 plaques—consistent with the known presence of such deposits in older monkeys (Uno & Walker, 1993; Sani et al., 2003) (upper panel, Figure 3B). However, the aged monkey exhibited a significantly higher abundance of Aβ42 plaques in the hippocampus injected with AAV-BRI-Aβ42 (lower panel, Figure 3B). Quantification of the number of Aβ42 plaques confirmed the age-dependent increase in Aβ42 plaque formation (n = 3 animals per group; 3 random slices were counted for each animal) (Figure 3C).

Microglial activation is a pathological hallmark of AD (Bartels et al., 2020). Double immunofluorescent staining revealed that in the hippocampus of the aged monkey, there were more microglia labeled by anti-IBA1, corresponding to the increased number of Aβ42 plaques (Figure 3D-E). Western blotting showed that Aβ42 did not alter the expression of neuronal proteins including NeuN ($P>0.05$), PSD95 ($P>0.05$), and SNAP25 ($P>0.05$) in the young monkeys, but it reduced NeuN expression in the aged monkeys, compared to the AAV-Control injected hippocampus (n=3 per group) (Figure 3F). The hippocampal microglia marker IBA1 ($P<0.001$) and astrocyte marker GFAP ($P<0.05$) are elevated in the young monkey group, and the IBA1 ($P<0.05$) also increased in the aged monkey, compared to the corresponding control group (n=3 per group) (Figure 3F). Aβ42 is found to be capable of triggering phosphorylated Tau in the brains (Price & Morris, 1999; Wang et al., 2016; Hanseeuw et al., 2019). While transgenic Aβ42 mouse models do not typically develop true neurofibrillary tangles (NFTs), a hallmark of AD pathology in humans (Jankowsky & Zheng, 2017), we observed that Aβ42 overexpression could increase the number of phosphorylated Tau-positive (AT8) cells, with this increase being much more pronounced in the hippocampus of aged monkeys (Figure 3G, H). These findings suggest that

Aβ42-mediated neuropathology in the non-human primate brain is more pronounced in aged monkeys, aligning with the age-dependent neuropathology observed in humans.

We then performed bilateral injection of the hippocampus with AAV-Aβ42 or AAV-control (10 μl, 1×10^13 vg/mL per side) into the hippocampus of monkeys (22–25 years of age) to examine their behaviors. We evaluated the learning ability of control and AAV-Aβ42-injected monkeys at various time points post-injection. Training the monkeys to complete cognitive tasks was challenging. Although AAV-Aβ42-injected monkeys showed trends toward worse performance in working memory and object reversal learning, no statistically significant differences were detected, even 12 months post-injection (Supplementary Figure S1A). Assessment of home cage activity revealed a decrease in daytime (light phase) activity with no change in nighttime (dark phase) activity in the AAV-Aβ42 group (Supplementary Figure S1B). By 12 months, these monkeys also exhibited a higher frequency of wake bouts, suggesting sleep disturbances compared to controls (Supplementary Figure S1C). Since sleep dysfunction is a recognized symptom in AD patients (Brzecka et al., 2018; Lacerda et al., 2024), our findings suggest that AAV-Aβ42-induced hippocampal dysfunction may contribute to AD-related sleep impairments. MRI analysis revealed that 12 months post-injection, the size of the hippocampal region in the AAV-Aβ42-injected monkeys appeared to be smaller than before the injection (Supplementary Figure S2). However, quantifying the size of the hippocampus in MRI can be challenging if the size is not dramatically altered. Therefore, we opted to use [^{11}C]PIB (Pittsburgh Compound B) PET imaging, a diagnostic tool that can visualize and quantify β-amyloid plaques in the human brain for the assessment of AD (Ruan & Sun, 2023; Lopresti et al., 2025). When comparing with an AAV-Control monkey using [^{11}C]PIB imaging, we observed increased signals in the hippocampus of the AAV-Aβ42 monkey (Supplementary Figure S3A, B).

In light of the potential impact of Aβ42 dosage on the phenotypes of monkeys, we proceeded to inject a larger volume of AAV (45 μl 1x10^{13} vg/mL per side) into the hippocampus of an additional three young (7 years) and three aged (26-28 years) monkeys, focusing on neuropathological changes in the aged monkeys and age-related molecular alterations at the single-cell level. The use of unilateral injections (AAV-Control vs. AAV-Aβ42) provides a rigorous internal control, minimizing inter-individual variability, while the inclusion of both young and aged cohorts is essential to demonstrate age-dependent effects. Twelve weeks after the injection, these animals were euthanized to isolate their hippocampi for histological and single-cell RNA sequencing analysis. In the hippocampus of aged monkeys, transgenic Aβ42 led to the formation

of more abundant plaques compared to the control monkey hippocampus (Figure 4A). Double immunostaining revealed a significant increase in microglial and astrocytic cells in the hippocampus (CA3 region) of the AAV-Aβ42 monkey compared to the control monkey (upper and middle panels in Figure 4B). Importantly, there was a decrease in NeuN-positive cells in the AAV-Aβ42-expressing hippocampus (lower panel in Figure 4B). Quantification of glial and neuronal cells confirmed that Aβ42 expression resulted in an increased number of microglial ($P<0.01$, n=3 per group) and astrocytic cells ($P<0.01$, n=3 per group) and a decreased number of NeuN-positive cells ($P<0.01$, n=3 per group) (Figure 4C).

Reduction of microglia in the hippocampus of aged monkeys

The difference in Aβ42 influence between young and aged monkeys prompted us to explore the underlying mechanism of Aβ42 neural toxicity with aging at single-cell resolution. We performed unilateral injections of AAV-Control and AAV-Aβ42 virus into the left and right hippocampi, respectively, of young (7 years) and aged (26–28 years) monkeys (4 groups, n=3 per group). To obtain a more comprehensive infection, each hippocampus was injected at three points (anterior, middle, and caudal; 15 μL per point, 1×10^{13} vg/mL). After three months post-injection, the hippocampal tissues of the injected sites were collected and mixed for single-nucleus RNA sequencing. After removing low-quality cells and performing batch correction with Harmony, we collected 86 353 cells in total from 12 samples across the 4 groups, and each group contained similar number of cells (20,673 cells for the young AAV-Control group, 21,071 cells for the young AAV-Aβ42 group; 20,120 cells for the aged AAV-Control group, 24,489 cells for the aged AAV-Aβ42 group) (Figure 5A, B). In total, we identified and clustered cells into 10 primary types based on their highly expressed markers, including excitatory neurons (*CAMK2A*, *SLC17A7*), inhibitory neurons (*GAD1*, *GAD2*), oligodendrocytes (*MOG*, *ST18)*, oligodendrocyte precursor cells (OPCs) (*PDGFRA*, *VCAN*), astrocytes (*GLI3*, *F3*), microglia (*C3*, *WDFY4*), fibroblasts (*EBF1*), epithelial cells (*DNAH12*), B cells (*EAF2*), and T cells (*ETS1*) (Supplementary Figure S4A-C). The excitatory neurons (36.28%), oligodendrocytes (32.47%), and microglia (21.51%) are the top three abundant cell types in our sequencing data. In both young and aged monkeys, we found that the proportion of excitatory neurons decreased (from 48.34% to 25.8% in young, from 50.70% to 22.00% in aged) after AAV-Aβ42 injection compared to the AAV-Control, which was similar to our previous western blot and immunofluorescent staining data. Interestingly, although the microglia proportion was elevated in the AAV-Aβ42 group compared to the AAV-

Control group in young (from 29.95% to 40.28%) and aged monkeys (from 5.17% to 9.75%), the overall microglia population showed a decline in the aged hippocampus (Figure 5C).

Microglia regulate cerebral immune responses and play a critical role in Aβ plaque clearance (Bartels et al., 2020; Lewcock et al., 2020). To investigate age-related differences in microglial function, we analyzed their transcriptional heterogeneity in young versus aged monkeys. We identified six distinct microglial subclusters—M1 (PPP2R2B/IL1RAPL1/PDE4B), M2 (APOE/FTH1/CD74), M3 (IQGAP2/DPYD/GPNMB), M4 (RBFOX1/CSMD1/LRP1B), M5 (SH3RF3/PLAC8/C3), and M6 (ST6GALNAC3/MERTK/SORL1)—and annotated them based on functional hallmarks: Homeostatic (M6), inflammatory (M5), anti-inflammatory (M4), DAM I (M2), DAM II-1 (M1), and DAM II-2 (M3) (Figure 5D-E, Supplementary Figure5A-C). Consistent with previous reports (Keren-Shaul et al., 2017; Gao et al., 2024), DAM I (M2) and DAM II (M1/M3) clusters exhibited elevated expression of key markers—APOE/CTSD/FTH1 and CTSL/CADM1/CD9/LGALS3, respectively (Supplementary Figure S5C). Notably, DAM II-1 and DAM II-2 displayed divergent transcriptional profiles: DAM II-2 showed upregulation of complement and inflammation-related pathways but downregulation of KRAS and DNA repair pathways compared to DAM II-1 (Figure 5F-G, Supplementary Figure S3B), suggesting functional specialization. The homeostatic microglia were the most abundant (29.2%), followed by DAM II-2 (17.9%) and DAM II-1 (14.4%) (Figure 5D). Intriguingly, hippocampal DAM II-2 microglia were elevated in young Aβ42-treated monkeys (19.5%) versus controls (11.8%), but this population declined sharply in aged groups (Control: 8.1%; Aβ42: 0.8%), and this difference was consistent across all biological replicates (Figure 5H, I). DAM II-2 microglia exhibit elevated GPNMB expression, a well-established biomarker linked to multiple neurodegenerative diseases, including Alzheimer's disease (AD), Parkinson's disease (PD), and amyotrophic lateral sclerosis (ALS), and the GPNMB-positive microglia show enhanced phagocytic activity (Hüttenrauch et al., 2018; Neal et al., 2018; Bogacki al., 2025). To further validate age-dependent microglial changes, we compared IBA1 (a pan-microglial marker) and GFAP (an astrocyte marker) expression in young versus aged WT monkey hippocampi. IBA1 levels decreased with age, whereas GFAP alteration is not significant (Figure 5J, M). Also, to further validate hippocampal IBA1 changes in young and aged monkeys, we performed IBA1 immunostaining in AAV–Aβ42 injected young and aged monkey brains. The results showed an approximately 30% decrease in IBA1-positive cells in the aged group compared with the young group, which is consistent with the Western blot findings (Figure 5K, L). The partial decrease in IBA1 expression aligns with the reduction in the DAM II-2

cluster observed in snRNA-seq data, pointing to an age-related loss of a specific microglial subtype in the hippocampus.

Selective vulnerability of monkey hippocampal neurons to Aβ42 toxicity

Although excitatory pyramidal cells (PCs) in the CA1 and CA3 regions are vulnerable in AD, the specific PC subtypes most sensitive to Aβ42 toxicity in primates remain unclear, largely due to the challenge of obtaining early-stage AD human brain samples. To address this, we analyzed monkey brains using established markers—PROX1/NPY1R for granule cells (GCs) and HS3ST4/PDE4B for PCs (Lavado et al., 2010; Castro et al., 2010; Madroñal et al., 2016; Ayhan et al., 2021)—and identified two GC subclusters (GCs_1 and GCs_2) and five PC subclusters: PCs_0 (TRPS1/RELN/TRHDE), PCs_1 (RAI4/KIAA1217), PCs_2 (CHST8/LMO1/NDST4), PCs_3 (CNTN6/SULF1), and PCs_4 (ABCA12/SLC38A11) (Figure 6A-C, Supplementary Figure S6A-F). Among these, PCs_0 was the dominant subtype in the young (82.67%) and aged control (67.97%) groups, as well as in young Aβ42-treated monkeys (68.71%). Strikingly, this population nearly vanished in aged Aβ42 monkeys (0.85%) (Figure 6B, D). Further characterization revealed that PCs_0 highly expressed TRPS1 (Figure 6D, E), a transcription factor (TF) linked to skeletal development (Georgescu et al., 2024) and recently detected in cortical astrocytes of mice (Natarajan et al., 2025) and in human neurons (Ayhan et al., 2021). TRPS1 is a key transcription factor that interacts with multiple signaling pathways, including Wnt and Hippo, and has been implicated in regulating cellular proliferation and survival. However, its role in neuronal cells remains unclear (Fantauzzo et al., 2011; Elster et al., 2018).

Aβ42 expression induced pronounced transcriptional changes in aged hippocampal PCs_0 compared to young groups (Figure 6F). Consistent with snRNA-seq data, TRPS1 expression was selectively reduced in excitatory neurons of the aged AAV-Aβ42 monkeys (Figure 6G), and immunofluorescence confirmed fewer TRPS1^{+} neurons in the Aβ42-treated aged hippocampus versus controls (Figure 6H, I). In summary, our findings reveal two key age- and Aβ42-dependent vulnerabilities: (1) a decline in DAM II microglia with aging, and (2) the selective loss of TRPS1^{+}RELN^{+} pyramidal neurons in the aged hippocampus under Aβ42 toxicity.

DISCUSSION

Although the pathological hallmarks of AD—Aβ deposition and hyperphosphorylated Tau—are well established, the mechanisms driving AD pathogenesis remain incompletely understood. Due to their close physiological and genetic similarity to humans, non-human primates (NHP) have been used to model AD and to investigate AD-related pathology (Li et al., 2020; Pan et al., 2024). Germline transgenic APP models have been developed (Chan et al., 2022; Li et al., 2024), but these require extended timeframes to develop AD neuropathology. Given the stronger association of Aβ and Tau pathology with AD progression, several studies have instead generated NHP models expressing synthetic Aβ (Beckman et al., 2019; Gary et al., 2019; Lam et al., 2021; Yue et al., 2021; He et al., 2025b), transgenic Tau (Tu et al., 2023; Jiang et al., 2024), or synthetic Tau seeds (Beckman et al., 2021, 2024; Darricau et al., 2024) in brain regions of non-human primates. In our study, AAV-mediated expression of BRI-Aβ was restricted to the hippocampus in monkeys of different ages. Unlike BRI-Aβ transgenic mouse models, which exhibit only mild synaptic dysfunction (Lawlor et al., 2007; Forner et al., 2019), our macaque model displays overt neuronal death. This pathological difference may stem from phylogenetic divergence between rodents and primates, including differences in lifespan, brain size and structure, and neuroimmune responses. Our approach provides a stable, long-term source of toxic Aβ while reducing variability associated with synthetic peptide preparations. Our findings demonstrate age-dependent neuropathological and molecular changes in Aβ42-expressing monkeys, offering new insights into hippocampal dysfunction in AD.

In this study, we investigated the effects of Aβ42 on the hippocampus of cynomolgus monkeys, given its critical role in memory function—a key domain impaired in AD-associated dementia. Despite the challenges of cognitive testing NHPs, we identified highly relevant reductions in daytime activity and sleep disturbances—non-cognitive behavioral phenotypes common in AD. Furthermore, aged animals exhibited more severe Aβ aggregation and pTau expression. This age-dependent pathology mirrors observations in AD patients and aligns with prior NHP studies demonstrating that aging potentiates Aβ-induced neuropathology (Yue et al., 2021; He et al., 2025b). Notably, snRNA-seq revealed an age-dependent reduction in hippocampal microglia in aged monkeys. Microglial dysfunction is increasingly recognized as a key contributor to AD and other neurodegenerative diseases, making it a promising therapeutic target (Bartels et al., 2020; Lewcock et al., 2020). While age-related microglial alterations have been reported in rodent AD models (Ogura et al., 1994; Deng et al., 2006; Antignano et al., 2023) and single-cell studies have characterized microglial heterogeneity in aging mice (Hammond et

al., 2019; Safaiyan et al., 2021; Wang et al., 2025; Sun et al., 2025), none have identified this specific decline in microglial numbers—a finding uniquely captured here in NHPs.

In our study, we found that the proportion of DAM II-2 subtype microglia was decreased in aged monkeys, and that expression of the DAM II-2 microglial marker GPNMB was also reduced in the aged hippocampus compared to the young monkeys following AAV-Aβ42 injection. Interestingly, GPNMB has been reported to be elevated across multiple neurodegenerative diseases(Hüttenrauch et al., 2018; Neal et al., 2018; Bogacki al., 2025), and its concentration in CSF is generally positively correlated with diverse disease progression (Aichholzer, et al., 2021; Doroszkiewicz et al., 2023). Several studies indicate that GPNMB can mediate cellular phagocytosis function, overexpression of GPNMB in microglia could enhance the clearance capacity for Aβ42 plaques (Wallings, et al., 2025; Liu et al., 2025). Thus, we speculate that the reduction of DAM II-2 microglia, or an age-related impairment in the transition from homeostatic to DAM II-2 microglia, may diminish cerebral Aβ42 clearance ability then increasing Aβ deposition and exacerbating Aβ42 toxicity. While the hippocampus maintains conserved anatomical features across mammalian species (Manns & Eichenbaum, 2006), primates display unique organizational characteristics that differentiate them from rodents (Ayhan et al., 2021) and should provide more clinically relevant insights into AD pathogenesis.

The age-dependent decline in hippocampal microglial function has been linked to aging-related memory impairment (Rim et al., 2024). For instance, selective clearance of senescent microglia in aged mice reverses cognitive deficits (Zhang et al., 2022). Similarly, in Tau-P301S mice (a tauopathy model), eliminating senescent glial cells—including microglia—reduces tau pathology, mitigates neurodegeneration, and improves cognitive function (Bussian et al., 2018). Unlike neurons, glial cells retain some regenerative capacity through adult gliogenesis. During development, microglial progenitors derived from yolk sac hematopoietic stem cells migrate into the brain parenchyma before blood-brain barrier (BBB) formation (Nayak et al., 2014). These cells mature and persist throughout life (Fuger et al., 2017), and microglial function is important for maintaining neurogenesis (Fang et al., 2023) and synaptic plasticity (Werneburg et al., 2017). While lost microglia may be partially replenished through resident cell proliferation, peripheral monocytes can also infiltrate to occupy vacant niches (Cronk et al., 2018). Notably, systemic factors influence this process: old blood plasma administration impairs hippocampal neurogenesis, reduces synaptic plasticity, induces microgliosis, and compromises learning and memory in mice (Villeda et al., 2011). These findings collectively underscore the role of

hippocampal microglial senescence in mediating age-related functional decline and posit it as a novel therapeutic target for cognitive restoration.

Microglia play a critical role in clearing misfolded proteins, including Aβ; however, their phagocytic capacity becomes impaired with age (Yoo et al., 2021). Although it remains to be investigated why hippocampal DAM II-2 microglia are particularly susceptible to aging, their reduction likely impairs the clearance of Aβ42 and increases neuronal vulnerability. Consistent with this, our findings demonstrate an age-dependent reduction of microglia in the hippocampus, leading to a more pronounced accumulation of toxic Aβ in aged versus young monkeys. This increased Aβ burden subsequently drives neurodegeneration, as evidenced by the selective loss of the neuronal cluster TRPS1^{+} PCs_0.1 compared to age-matched controls. As a transcription factor, TRPS1 regulates a complex transcriptional network rather than a single pathway. Several studies have shown that TRPS1 influences cellular progenitor development by modulating the WNT signaling pathway during hair follicle (vibrissa) morphogenesis and affects cell proliferation and survival by suppressing Yes-associated protein (YAP) activity in the Hippo pathway in breast cancer cells (Fantauzzo et al., 2012; Elster et al., 2018). Interestingly, a recent genome-wide association study (GWAS) in African Americans (AAs) identified a strong association between the TRPS1 variant *rs16885997* and cognitive decline (P=2.52 × 10^{-7}), which was only behind an *APOE* variant (P=1.92 × 10^{-14}) in significance (Raj et al., 2016). This finding suggests a potential link between TRPS1 dysregulation and Alzheimer's disease pathogenesis. However, the function of the TRPS1^{+} PCs_0.1 neuronal population has yet to be fully elucidated, but its loss—combined with age-related microglial decline—may synergistically exacerbate hippocampal dysfunction, ultimately contributing to the dementia phenotype in AD. Thus, using a non-human primate model, our study demonstrates that Aβ42 toxicity is exacerbated in the aged primate hippocampus due to a combination of microglial decline and the selective vulnerability of a specific neuronal subtype (TRPS1+ PCs_0.1). These findings also identify a new potential therapeutic target for treating AD phenotypes.

Our study also has several limitations that warrant future investigation. First, due to the central role of female monkeys in reproductive programs, they are typically maintained for longer periods than males, and female animals generally exhibit more pronounced AD-related pathology than males (Yang et al., 2018; Dennison et al., 2021; Poon et al., 2023). Therefore, we used only female animals in our experiments. Although these aged animals developed distinct and severe

AD-related pathologies after AAV-Aβ42 injection, including Aβ plaques, pTau tangles, and neuronal loss, future work should include male animals to determine if there is sex-dependent pathology in the aged monkey hippocampus. Second, we observed that TRPS1+ pyramidal neurons were more sensitive to Aβ toxicity in the aged hippocampus, but the underlying mechanism requires further investigation. Third, the direct relationship between DAM II-2 microglia and Aβ in the monkey hippocampus was not fully explored in this study. Future work should determine whether DAM II-2 microglia indeed exhibit an enhanced capacity to clear Aβ plaques compared with other microglial subtypes. In addition, the mechanisms responsible for the age-related reduction in DAM II-2 microglia also require further study.

COMPETING INTERESTS

The authors declare that they have no competing interests.

DATA AVAILABILITY

The scRNA-seq data generated in this study were deposited in the SRA database (PRJNA1456348), Science Data Bank (DOI:10.57760/sciencedb.j00139.00284), and the processed data could be found in GEO database (GSE330450).

AUTHORS' CONTRIBUTIONS

X.L., designed and supervised the research experiments. L. C. analyzed snRNAseq data, J Z, Z.W. and B.L. established and analyzed monkey models. Y.L., X.S., K.C., performed molecular biology and histological studies. B. L., W. Y., H. X. and L. W analyzed brain imaging results. X. L. wrote the manuscript. S. Y., S. L. W. L, and X.W. provided advice or reagents and edited the manuscript. All authors read and approved the final version of the manuscript.

FUNDING SOURCES

This work was supported by The National Natural Science Foundation of China (82394422, 82371874, U24A6013, 82271902, 82171244, 32370567, 82371178), the National Key Research and Development Program by the Ministry of Science and Technology (2021YFA0805300, 2021YFA0805203), and the Department of Science and Technology of Guangdong Province (2021ZT09Y007; 2020B121201006).

ACKNOWLEDGMENTS

We thank Yan Zhou and Xuntao Yin for providing MRI scanning and analysis. We thank Guangdong Landao Biotechnology Co. Ltd for providing animal facility and animal care.

REFERENCES

Aichholzer F, Klafki HW, Ogorek I, Vogelgsang J, Wiltfang J, Scherbaum N, et al. Evaluation of cerebrospinal fluid glycoprotein NMB (GPNMB) as a potential biomarker for Alzheimer's disease. Alzheimers Res Ther. 2021;13(1):94. DOI: 10.1186/s13195-021-00828-1.

Antignano I, Liu Y, Offermann N, Capasso M. Aging microglia. Cell Mol Life Sci. 2023 Apr 21;80(5):126. DOI: 10.1007/s00018-023-04775-y.

Ayhan F, Kulkarni A, Berto S, Sivaprakasam K, Douglas C, Lega BC, Konopka G. Resolving cellular and molecular diversity along the hippocampal anterior-to-posterior axis in humans. Neuron. 2021 Jul 7;109(13):2091-2105.e6. DOI: 10.1016/j.neuron.2021.05.003.

Bartels T, De Schepper S, Hong S. Microglia modulate neurodegeneration in Alzheimer's and Parkinson's diseases. Science. 2020 Oct 2;370(6512):66-69. DOI: 10.1126/science.abb8587.

Beckman D, Ott S, Donis-Cox K, Janssen WG, Bliss-Moreau E, Rudebeck PH, Baxter MG, Morrison JH. Oligomeric Aβ in the monkey brain impacts synaptic integrity and induces accelerated cortical aging. Proc Natl Acad Sci U S A. 2019 Dec 26;116(52):26239-26246. DOI: 10.1073/pnas.1902301116.

Beckman D, Chakrabarty P, Ott S, Dao A, Zhou E, Janssen WG, Donis-Cox K, Muller S, Kordower JH, Morrison JH. A novel tau-based rhesus monkey model of Alzheimer's pathogenesis. Alzheimers Dement. 2021 Jun;17(6):933-945. DOI: 10.1002/alz.12318.

Beckman D, Diniz GB, Ott S, Hobson B, Chaudhari AJ, Muller S, Chu Y, Takano A, Schwarz AJ, Yeh CL, McQuade P, Chakrabarty P, Kanaan NM, Quinton MS, Simen AA, Kordower JH, Morrison JH. Temporal progression of tau pathology and neuroinflammation in a rhesus monkey model of Alzheimer's disease. Alzheimers Dement. 2024 Aug;20(8):5198-5219. DOI: 10.1002/alz.13868.

Bogacki EC, Parfitt GM, Cunha A, Longmore G, Wray S, Lewis PA, et al. GPNMB is a biomarker for lysosomal dysfunction and is secreted via LRRK2-modulated lysosomal exocytosis. Sci Adv. 2025;11(51):eadv1434. DOI: 10.1126/sciadv.adv1434.

Brzecka, Anna et al. “Sleep Disorders Associated With Alzheimer's Disease: A Perspective.” Frontiers in neuroscience vol. 12 330. 31 May. 2018. DOI: 10.3389/fnins.2018.00330.

Bussian TJ, Aziz A, Meyer CF, Swenson BL, van Deursen JM, Baker DJ. Clearance of senescent glial cells prevents tau-dependent pathology and cognitive decline. Nature. 2018 Oct;562(7728):578-582. DOI: 10.1038/s41586-018-0543-y.

Butler A, Hoffman P, Smibert P, Papalexi E, Satija R. Integrating single-cell transcriptomic data across different conditions, technologies, and species. Nat Biotechnol. 2018 Jun;36(5):411-420. doi: 10.1038/nbt.4096. DOI: 10.1038/nbt.4096.

Castro JE, Varea E, Márquez C, Cordero MI, Poirier G, Sandi C. Role of the amygdala in antidepressant effects on hippocampal cell proliferation and survival and on depression-like behavior in the rat. PLoS One. 2010 Jan 8;5(1):e8618. DOI: 10.1371/journal.pone.0008618.

Chan AWS, Cho IK, Li CX, Zhang X, Patel S, Rusnak R, Raper J, Bachevalier J, Moran SP, Chi T, Cannon KH, Hunter CE, Martin RC, Xiao H, Yang SH, Gumber S, Herndon JG, Rosen RF, Hu WT, Lah JJ, Levey AI, Smith Y, Walker LC. Cerebral Aβ deposition in an Aβ-precursor protein-transgenic rhesus monkey. Aging Brain. 2022;2:100044. DOI: 10.1016/j.nbas.2022.100044.

Chang CW, Shao E, Mucke L. Tau: Enabler of diverse brain disorders and target of rapidly evolving therapeutic strategies. Science. 2021 Feb 26;371(6532):eabb8255. DOI: 10.1126/science.abb8255.

Chen, Y., Yu, J., Niu, Y., Qin, D., Liu, H., Li, G., Hu, Y., Wang, J., Lu, Y., Kang, Y., et al. (2017). Modeling Rett Syndrome Using TALEN-Edited MECP2 Mutant Cynomolgus Monkeys. Cell 169, 945-955 e910. DOI: 10.1016/j.cell.2017.04.035.

Cole SL, Vassar R. The Alzheimer's disease beta-secretase enzyme, BACE1. Mol Neurodegener. 2007 Nov 15;2:22. DOI: 10.1186/1750-1326-2-22.

Cronk JC, Filiano AJ, Louveau A, Marin I, Marsh R, Ji E, Goldman DH, Smirnov I, Geraci N, Acton S, Overall CC, Kipnis J. Peripherally derived macrophages can engraft the brain independent of irradiation and maintain an identity distinct from microglia. J Exp Med. 2018 Jun 4;215(6):1627-1647. DOI: 10.1084/jem.20180247.

Darricau M, Dou C, Kinet R, Zhu T, Zhou L, Li X, Bedel A, Claverol S, Tokarski C, Katsinelos T, McEwan WA, Zhang L, Gao R, Bourdenx M, Dehay B, Qin C, Bezard E, Planche V. Tau seeds from Alzheimer's disease brains trigger tau spread in macaques while oligomeric-Aβ mediates pathology maturation. Alzheimers Dement. 2024 Mar;20(3):1894-1912. DOI: 10.1002/alz.13604.

Deng XH, Bertini G, Xu YZ, Yan Z, Bentivoglio M. Cytokine-induced activation of glial cells in the mouse brain is enhanced at an advanced age. Neuroscience. 2006 Aug 25;141(2):645-671. DOI: 10.1016/j.neuroscience.2006.04.016.

Doroszkiewicz J, Kulczyńska-Przybik A, Dulewicz M, Borawska R, Zajkowska M, Słowik A, et al. Potential utility of cerebrospinal fluid glycoprotein nonmetastatic melanoma protein B as a neuroinflammatory diagnostic biomarker in mild cognitive impairment and Alzheimer's disease. J Clin Med. 2023;12(14):4689. DOI: 10.3390/jcm12144689.

Elster D, Tollot M, Schlegelmilch K, Ori A, Rosenwald A, Sahai E, et al. TRPS1 shapes YAP/TEAD-dependent transcription in breast cancer cells. Nat Commun. 2018;9(1):3115. DOI: 10.1038/s41467-018-05370-7.

Fang S, Wu Z, Guo Y, Zhu W, Wan C, Yuan N, Chen J, Hao W, Mo X, Guo X, Fan L, Li X, Chen J. Roles of microglia in adult hippocampal neurogenesis in depression and their therapeutics. Front Immunol. 2023 Oct 10;14:1193053. DOI: 10.3389/fimmu.2023.1193053.

Fantauzzo JR, Eichenbaum H. Evolution of declarative memory. Hippocampus. 2006;16(9):795-808. DOI: 10.1002/hipo.20205.

Fantauzzo KA, Kurban M, Levy B, Christiano AM. Trps1 and its target gene Sox9 regulate epithelial proliferation in the developing hair follicle and are associated with hypertrichosis. PLoS Genet. 2012;8(11):e1003002. DOI: 10.1371/journal.pgen.1003002.

Forner S, Martini AC, Prieto GA, Dang CT, Rodriguez-Ortiz CJ, Reyes-Ruiz JM, et al. Intra- and extracellular β-amyloid overexpression via adeno-associated virus-mediated gene transfer impairs memory and synaptic plasticity in the hippocampus. Sci Rep. 2019;9(1):15936. DOI: 10.1038/s41598-019-52324-0.

Füger P, Hefendehl JK, Veeraraghavalu K, Wendeln AC, Schlosser C, Obermüller U, Wegenast-Braun BM, Neher JJ, Martus P, Kohsaka S, Thunemann M, Feil R, Sisodia SS, Skodras A, Jucker M. Microglia turnover with aging and in an Alzheimer's model via long-term in vivo single-cell imaging. Nat Neurosci. 2017 Oct;20(10):1371-1376.

Gao C, Jiang J, Tan Y, Chen S. Microglia in neurodegenerative diseases: mechanism and potential therapeutic targets. Signal Transduct Target Ther. 2023 Sep 22;8(1):359. DOI: 10.1038/s41392-023-01588-0.

Gary C, Lam S, Hérard AS, Koch JE, Petit F, Gipchtein P, Sawiak SJ, Caillierez R, Eddarkaoui S, Colin M, Aujard F, Deslys JP; French Neuropathology Network; Brouillet E, Buée L, Comoy EE, Pifferi F, Picq JL, Dhenain M. Encephalopathy induced by Alzheimer brain inoculation in a non-human primate. Acta Neuropathol Commun. 2019 Sep 4;7(1):126. DOI: 10.1186/s40478-019-0771-x.

Georgescu AC, Georgescu TA, Duca-Barbu SA, Pop LG, Toader DO, Suciu N, Cretoiu D. A Comprehensive Review of TRPS1 as a Diagnostic Immunohistochemical Marker for Primary Breast Carcinoma: Latest Insights and Diagnostic Pitfalls. Cancers (Basel). 2024 Oct 23;16(21):3568. DOI: 10.3390/cancers16213568.

Goate A, Chartier-Harlin MC, Mullan M, Brown J, Crawford F, Fidani L, Giuffra L, Haynes A, Irving N, James L, et al. Segregation of a missense mutation in the amyloid precursor protein gene with familial Alzheimer's disease. Nature. 1991 Feb 21;349(6311):704-6. DOI: 10.1038/349704a0.

Goedert M, Spillantini MG. A century of Alzheimer's disease. Science. 2006 Nov 3;314(5800):777-81. DOI: 10.1126/science.1132814.

Hammond TR, Dufort C, Dissing-Olesen L, Giera S, Young A, Wysoker A, Walker AJ, Gergits F, Segel M, Nemesh J, Marsh SE, Saunders A, Macosko E, Ginhoux F, Chen J, Franklin RJM, Piao X, McCarroll SA, Stevens B. Single-Cell RNA Sequencing of Microglia throughout the Mouse Lifespan and in the Injured Brain Reveals Complex Cell-State Changes. Immunity. 2019 Jan 15;50(1):253-271.e6. DOI: 10.1016/j.immuni.2018.11.004.

Han R, Wang Q, Xiong X, Chen X, Tu Z, Li B, Zhang F, Chen C, Pan M, Xu T, Chen L, Wang Z, Liu Y, He D, Guo X, He F, Wu P, Yin P, Liu Y, Yan X, Li S, Li XJ, Yang W. Deficiency of parkin causes neurodegeneration and accumulation of pathological α-synuclein in monkey models. J Clin Invest. 2024 Oct 15;134(20):e179633. DOI: 10.1172/JCI179633.

Hanseeuw, B.J., Betensky, R.A., Jacobs, H.I.L., Schultz, A.P., Sepulcre, J., Becker, J.A., Cosio, D.M.O., Farrell, M., Quiroz, Y.T., Mormino, E.C., et al. (2019). Association of Amyloid and Tau With Cognition in Preclinical Alzheimer Disease: A Longitudinal Study. JAMA Neurol. Published online June 3, 2019. DOI: 10.1001/jamaneurol.2019.1424.

Hardy J. The discovery of Alzheimer-causing mutations in the APP gene and the formulation of the "amyloid cascade hypothesis". FEBS J. 2017 Apr;284(7):1040-1044.

He F, Shi WJ, Liu W, Fan JX, He ZG, Zhang YQ, Xiao J, Ruan WW, Gai YK, Zhang HL, Yang BB, Qin Y, Wang H, Li J, Wang JL, Liu S, Shi LP, Chen ZX, Jiang WJ, An N, Xue PJ, Wang ZH, Yang RJ, Tian PY, Chen Z, Xiao L, Yang ZS, Feng KB, Tan WY, Sun ZM, Xu W, Shu H, Wang JZ. A mass-producible macaque model displays a durable Alzheimer-like cognitive deficit and hallmark amyloid-β/tau/neurofilament light chain pathologies. J Alzheimers Dis. 2025b Jun;105(4):1432-1446. DOI: 10.1177/13872877251334316.

He Z, Zhang W, Chen P, Li S, Tao M, Yue F, Hong W, Feng S, Jing N. Amyloid-β oligomers drive amyloid deposit and cascaded tau pathology of Alzheimer's disease in aged brains of non-human primates. J Genet Genomics. 2025a Feb 25:S1673-8527(25)00052-9. DOI: 10.1016/j.jgg.2025.02.007.

Herndon JG, Moss MB, Rosene DL, Killiany RJ. Patterns of cognitive decline in aged rhesus monkeys. Behav Brain Res. 1997 Aug;87(1):25-34. DOI: 10.1016/S0166-4328(96)02256-5.

Hüttenrauch M, Ogorek I, Klafki H, Otto M, Stadelmann C, Weggen S, et al. Glycoprotein NMB: a novel Alzheimer's disease associated marker expressed in a subset of activated microglia. Acta Neuropathol Commun. 2018;6(1):108. DOI: 10.1186/s40478-018-0612-3.

Jankowsky JL, Zheng H. Practical considerations for choosing a mouse model of Alzheimer's disease. Mol Neurodegener. 2017 Dec 22;12(1):89. DOI: 10.1186/s13024-017-0231-7.

Jiang Z, Wang J, Qin Y, Liu S, Luo B, Bai F, Wei H, Zhang S, Wei J, Ding G, Ma L, He S, Chen R, Sun Y, Chen Y, Wang L, Xu H, Wang X, Chen G, Lei W. A nonhuman primate model with Alzheimer's disease-like pathology induced by hippocampal overexpression of human tau. Alzheimers Res Ther. 2024 Jan 27;16(1):22. DOI: 10.1186/s13195-024-01392-0.

Jucker M, Walker LC. Alzheimer's disease: From immunotherapy to immunoprevention. Cell. 2023 Sep 28;186(20):4260-4270. DOI: 10.1016/j.cell.2023.08.021.

Keren-Shaul H, Spinrad A, Weiner A, Matcovitch-Natan O, Dvir-Szternfeld R, Ulland TK, David E, Baruch K, Lara-Astaiso D, Toth B, Itzkovitz S, Colonna M, Schwartz M, Amit I. A Unique Microglia Type Associated with Restricting Development of Alzheimer's Disease. Cell. 2017 Jun 15;169(7):1276-1290.e17. DOI: 10.1016/j.cell.2017.05.018.

Kim J, Chakrabarty P, Hanna A, March A, Dickson DW, Borchelt DR, Golde T, Janus C. Normal cognition in transgenic BRI2-Aβ mice. Mol Neurodegener. 2013 May 12;8:15. DOI: 10.1186/1750-1326-8-15.

Korsunsky I, Millard N, Fan J, Slowikowski K, Zhang F, Wei K, Baglaenko Y, Brenner M, Loh PR, Raychaudhuri S. Fast, sensitive and accurate integration of single-cell data with Harmony. Nat Methods. 2019 Dec;16(12):1289-1296. DOI: 10.1038/s41592-019-0619-0.

Kshirsagar S, Alvir RV, Hindle A, Kumar S, Vijayan M, Pradeepkiran JA, Reddy AP, Ramasubramanian B, Reddy PH. Early Cellular, Molecular, Morphological and Behavioral Changes in the Humanized Amyloid-Beta-Knock-In Mouse Model of Late-Onset Alzheimer's Disease. Cells. 2022 Feb 19;11(4):733. DOI: 10.3390/cells11040733.

Lacerda, Rafael Antônio Vicente et al. “Sleep disorders and risk of alzheimer's disease: A two-way road.” Ageing research reviews vol. 101 (2024): 102514. DOI: 10.1016/j.arr.2024.102514.

Lai ZC, Moss MB, Killiany RJ, Rosene DL, Herndon JG. Executive system dysfunction in the aged monkey: spatial and object reversal learning. Neurobiol Aging. 1995 Nov-Dec;16(6):947-54. DOI: 10.1016/0197-4580(95)02014-4.

Lam S, Petit F, Hérard AS, Boluda S, Eddarkaoui S, Guillermier M; Brain Bank Neuro-C. E. B. Neuropathology Network; Buée L, Duyckaerts C, Haïk S, Picq JL, Dhenain M. Transmission of amyloid-beta and tau pathologies is associated with cognitive impairments in a primate. Acta Neuropathol Commun. 2021 Oct 12;9(1):165. DOI: 10.1186/s40478-021-01266-8.

Lavado A, Lagutin OV, Chow LM, Baker SJ, Oliver G. Prox1 is required for granule cell maturation and intermediate progenitor maintenance during brain neurogenesis. PLoS Biol. 2010 Aug 17;8(8):e1000460. DOI: 10.1371/journal.pbio.1000460.

Lawlor PA, Bland RJ, Das P, Price RW, Holloway V, Smithson L, et al. Novel rat Alzheimer's disease models based on AAV-mediated gene transfer to selectively increase hippocampal Abeta levels. Mol Neurodegener. 2007;2:11. DOI: 10.1186/1750-1326-2-11.

Levy, E., Carman, M.D., Fernandez-Madrid, I.J., Power, M.D., Lie- berburg, I., van Duinen, S.G., Bots, G.T., Luyendijk, W., and Frangi- one, B. (1990). Mutation of the Alzheimer’s disease amyloid gene in hereditary cerebral hemorrhage, Dutch type. Science 248, 1124– 1126. DOI: 10.1126/science.2111584.

Lewcock JW, Schlepckow K, Di Paolo G, Tahirovic S, Monroe KM, Haass C. Emerging Microglia Biology Defines Novel Therapeutic Approaches for Alzheimer's Disease. Neuron. 2020 Dec 9;108(5):801-821. DOI: 10.1016/j.neuron.2020.09.029.

Lewis PA, Piper S, Baker M, Onstead L, Murphy MP, Hardy J, Wang R, McGowan E, Golde TE. Expression of BRI-amyloid beta peptide fusion proteins: a novel method for specific high-level expression of amyloid beta peptides. Biochim Biophys Acta. 2001 Jul 27;1537(1):58-62. DOI: 10.1016/S0925-4439(01)00054-0.

Li B, Zhao H, Tu Z, Yang W, Han R, Wang L, Luo X, Pan M, Chen X, Zhang J, Xu H, Guo X, Yan S, Yin P, Zhao Z, Liu J, Luo Y, Li Y, Yang Z, Zhang B, Tan Z, Xu H, Jiang T, Jiang YH, Li S, Zhang YQ, Li XJ. CHD8 mutations increase gliogenesis to enlarge brain size in the nonhuman primate. Cell Discov. 2023 Mar 7;9(1):27. DOI: 10.1038/s41421-023-00525-3.

Li M, Guan M, Lin J, Zhu K, Zhu J, Guo M, Li Y, Chen Y, Chen Y, Zou Y, Wu D, Xu J, Yi W, Fan Y, Ma S, Chen Y, Xu J, Yang L, Dai J, Ye T, Lu Z, Chen Y. Early blood immune molecular alterations in cynomolgus monkeys with a PSEN1 mutation causing familial Alzheimer's disease. Alzheimers Dement. 2024 Aug;20(8):5492-5510. DOI: 10.1002/alz.14046.

Li ZH, He XP, Li H, He RQ, Hu XT. Age-associated changes in amyloid-β and formaldehyde concentrations in cerebrospinal fluid of rhesus monkeys. Zool Res. 2020 Jul 18;41(4):444-448. DOI: 10.24272/j.issn.2095-8137.2020.088.

Liu Y, Pang L, Khan F, Wu J, Zhou F, Horbinski C, et al. Glycoprotein NMB mediates bidirectional GSC-TAM interactions to promote tumor progression. JCI Insight. 2025;10(13):e187684. DOI: 10.1172/JCI187684.

Long JM, Holtzman DM. Alzheimer Disease: An Update on Pathobiology and Treatment Strategies. Cell. 2019 Oct 3;179(2):312-339. DOI: 10.1016/j.cell.2019.09.001.

Lopresti BJ, Cohen AD, DelBene A, Reese A, Matan C, Gogola A, Chiang M, Snitz BE, Laymon CM, Berman SB, Royse SK, Lopez OL, Villemagne VL. Comparison of visual and analytic methods of Alzheimer's disease pathologic staging. Alzheimers Dement. 2025 Jul;21(7):e70520. DOI: 10.1002/alz.70520.

Madroñal N, Delgado-García JM, Fernández-Guizán A, Chatterjee J, Köhn M, Mattucci C, Jain A, Tsetsenis T, Illarionova A, Grinevich V, Gross CT, Gruart A. Rapid erasure of hippocampal memory following inhibition of dentate gyrus granule cells. Nat Commun. 2016 Mar 18;7:10923. DOI: 10.1038/ncomms10923.

Makori N, Watson RE, Hogrefe CE, Lalayeva N, Oneda S. Object discrimination and reversal learning in infant and juvenile non-human primates in a non-clinical laboratory. J Med Primatol. 2013 Jun;42(3):147-57. DOI: 10.1111/jmp.12020.

McGinnis CS, Patterson DM, Winkler J, Conrad DN, Hein MY, Srivastava V, Hu JL, Murrow LM, Weissman JS, Werb Z, Chow ED, Gartner ZJ. MULTI-seq: sample multiplexing for single-cell RNA sequencing using lipid-tagged indices. Nat Methods. 2019 Jul;16(7):619-626. DOI: 10.1038/s41592-019-0424-0.

McGowan E, Pickford F, Kim J, Onstead L, Eriksen J, Yu C, Skipper L, Murphy MP, Beard J, Das P, Jansen K, DeLucia M, Lin WL, Dolios G, Wang R, Eckman CB, Dickson DW, Hutton M, Hardy J, Golde T. Abeta42 is essential for parenchymal and vascular amyloid deposition in mice. Neuron. 2005 Jul 21;47(2):191-199. DOI: 10.1016/j.neuron.2005.06.020.

Natarajan P, Koupourtidou C, de Resseguier T, Thorwirth M, Bocchi R, Fischer-Sternjak J, Gleiss S, Rodrigues D, Myoga MH, Ninkovic J, Masserdotti G, Götz M. Single Cell Deletion of the Transcription Factors Trps1 and Sox9 in Astrocytes Reveals Novel Functions in the Adult Cerebral Cortex. Glia. 2025 Apr;73(4):737-758. DOI: 10.1002/glia.24227.

Nayak D, Roth TL, McGavern DB. Microglia development and function. Annu Rev Immunol. 2014;32:367-402. DOI: 10.1146/annurev-immunol-032713-120240.

Neal ML, Boyle AM, Budge KM, Safadi FF, Richardson JR. The glycoprotein GPNMB attenuates astrocyte inflammatory responses through the CD44 receptor. J Neuroinflammation. 2018;15(1):73. DOI: 10.1186/s12974-018-1094-8.

Noser AE, Dai H, Marker AM, Raymond JK, Majidi S, Clements MA, Stanek KR, Patton SR. Parental depression and diabetes-specific distress after the onset of type 1 diabetes in children. Health Psychol. 2019 Feb;38(2):103-112. DOI: 10.1037/hea0000700.

Ogura K, Ogawa M, Yoshida M. Effects of ageing on microglia in the normal rat brain: immunohistochemical observations. Neuroreport. 1994 Jun 2;5(10):1224-6. DOI: 10.1097/00001756-199406020-00039.

Pan MT, Zhang H, Li XJ, Guo XY. Genetically modified non-human primate models for research on neurodegenerative diseases. Zool Res. 2024 Mar 18;45(2):263-274.

Price, J.L., and Morris, J.C. (1999). Tangles and plaques in nondemented ag-ing and “preclinical” Alzheimer’s disease. Ann. Neurol. 45, 358–368.

Rafii MS, Aisen PS. Amyloid-lowering immunotherapies for Alzheimer disease: current status and future directions. Nat Rev Neurol. 2025 Jul 21. doi: 10.1038/s41582-025-01123-5. DOI: 10.1038/s41582-025-01123-5.

Raj T, Chibnik LB, McCabe C, Wong A, Replogle JM, Yu L, et al. Genetic architecture of age-related cognitive decline in African Americans. Neurol Genet. 2016;3(1):e125. DOI: 10.1212/NXG.0000000000000125.

Rim C, You MJ, Nahm M, Kwon MS. Emerging role of senescent microglia in brain aging-related neurodegenerative diseases. Transl Neurodegener. 2024 Feb 20;13(1):10. DOI: 10.1186/s40035-024-00356-5.

Rovelet-Lecrux A, Hannequin D, Raux G, Le Meur N, Laquerrière A, Vital A, Dumanchin C, Feuillette S, Brice A, Vercelletto M, Dubas F, Frebourg T, Campion D. APP locus duplication causes autosomal dominant early-onset Alzheimer disease with cerebral amyloid angiopathy. Nat Genet. 2006 Jan;38(1):24-6. DOI: 10.1038/ng1746.

Ruan D, Sun L. Amyloid-β PET in Alzheimer's disease: A systematic review and Bayesian meta-analysis. Brain Behav. 2023 Jan;13(1):e2850. DOI: 10.1002/brb3.2850.

Safaiyan S, Besson-Girard S, Kaya T, Cantuti-Castelvetri L, Liu L, Ji H, Schifferer M, Gouna G, Usifo F, Kannaiyan N, Fitzner D, Xiang X, Rossner MJ, Brendel M, Gokce O, Simons M. White matter aging drives microglial diversity. Neuron. 2021 Apr 7;109(7):1100-1117.e10. DOI: 10.1016/j.neuron.2020.12.011.

Sani S, Traul D, Klink A, Niaraki N, Gonzalo-Ruiz A, Wu CK, Geula C. Distribution, progression and chemical composition of cortical amyloid-beta deposits in aged rhesus monkeys: similarities to the human. Acta Neuropathol. 2003 Feb;105(2):145-56. DOI: 10.1007/s00401-002-0633-4.

Shi J, Touchon J, Middleton LT, Rovira MB, Vassar R, Vellas B, Shen Y. Now and future: Strategies for diagnosis, prevention and therapies for Alzheimer's disease. Sci Bull (Beijing). 2024 Dec 15;69(23):3777-3784. DOI: 10.1016/j.scib.2024.12.013.

Sun ED, Nagvekar R, Pogson AN, Brunet A. Brain aging and rejuvenation at single-cell resolution. Neuron. 2025 Jan 8;113(1):82-108. DOI: 10.1016/j.neuron.2023.12.008.

Tanzi RE, Bertram L. Twenty years of the Alzheimer's disease amyloid hypothesis: a genetic perspective. Cell. 2005 Feb 25;120(4):545-55. DOI: 10.1016/j.cell.2005.02.045.

Tu Z, Zhao H, Li B, Yan S, Wang L, Tang Y, Li Z, Bai D, Li C, Lin Y, Li Y, Liu J, Xu H, Guo X, Jiang YH, Zhang YQ, Li XJ. CRISPR/Cas9-mediated disruption of SHANK3 in monkey leads to drug-treatable autism-like symptoms. Hum Mol Genet. 2019 Feb 15;28(4):561-571. DOI: 10.1093/hmg/ddz187.

Tu Z, Yan S, Han B, et al. Tauopathy promotes spinal cord-dependent production of toxic amyloid-beta in transgenic monkeys. Signal Transduct Target Ther 2023; 8: 358. DOI: 10.1038/s41392-023-01015-2.

Uno H, Walker LC. The age of biosenescence and the incidence of cerebral beta-amyloidosis in aged captive rhesus monkeys. Ann N Y Acad Sci. 1993; 695: 232-235. DOI: 10.1111/j.1749-6632.1993.tb18384.x.

Villeda SA, Luo J, Mosher KI, Zou B, Britschgi M, Bieri G, Stan TM, Fainberg N, Ding Z, Eggel A, Lucin KM, Czirr E, Park JS, Couillard-Després S, Aigner L, Li G, Peskind ER, Kaye JA, Quinn JF, Galasko DR, Xie XS, Rando TA, Wyss-Coray T. The ageing systemic milieu negatively regulates neurogenesis and cognitive function. Nature. 2011 Aug 31;477(7362):90-4. DOI: 10.1038/nature10357.

Wallings RL, Gillett DA, Staley HA, Mahn S, Mark J, Neighbarger N, et al. ASO-mediated knock-down of GPNMB in mutant-GRN and in Grn-deficient peripheral myeloid cells disrupts lysosomal function and immune responses. Mol Neurodegener. 2025;20(1):41. DOI: 10.1186/s13024-025-00711-3.

Wang, L., Benzinger, T.L., Su, Y., Christensen, J., Friedrichsen, K., Aldea, P., McConathy, J., Cairns, N.J., Fagan, A.M., Morris, J.C., et al. (2016). Evaluation of Tau Imaging in Staging Alzheimer Disease and Revealing Interactions Between b-Amyloid and Tauopathy. JAMA Neurol. 73, 1070–1077.

Wang Q, Zhu BT, Lei P. Animal models of Alzheimer's disease: Current strategies and new directions. Zool Res. 2024 Nov 18;45(6):1385-1407.

Wang X, Zhang H, Wan Z, Li X, Ibáñez CF, Xie M. A single-cell transcriptomic atlas of all cell types in the brain of 5xFAD Alzheimer mice in response to dietary inulin supplementation. BMC Biol. 2025 May 9;23(1):124. DOI: 10.1186/s12915-024-01814-2.

Werneburg S, Feinberg PA, Johnson KM, Schafer DP. A microglia-cytokine axis to modulate synaptic connectivity and function. Curr Opin Neurobiol. 2017 Dec;47:138-145. DOI: 10.1016/j.conb.2017.08.001.

Yoo HJ, Kwon MS. Aged Microglia in Neurodegenerative Diseases: Microglia Lifespan and Culture Methods. Front Aging Neurosci. 2022 Jan 5;13:766267. DOI: 10.3389/fnagi.2021.766267.

Yue F, Feng S, Lu C, Zhang T, Tao G, Liu J, Yue C, Jing N. Synthetic amyloid-β oligomers drive early pathological progression of Alzheimer's disease in nonhuman primates. iScience. 2021 Sep 30;24(10):103207. DOI: 10.1016/j.isci.2021.103207.

Zhang H, Pan MT, Li YX, Li XJ, Guo XY, He DJ. Understanding Tau pathology: Insights from animal models. Zool Res. 2025 Sep 18;46(5):1244-1258.

Zhang X, Pearsall VM, Carver CM, Atkinson EJ, Clarkson BDS, Grund EM, et al. Rejuvenation of the aged brain immune cell landscape in mice through p16-positive senescent cell clearance. Nat Commun. 2022;13(1):5671. DOI: 10.1038/s41467-022-33327-6.

Science Press
ZR Zoological Research

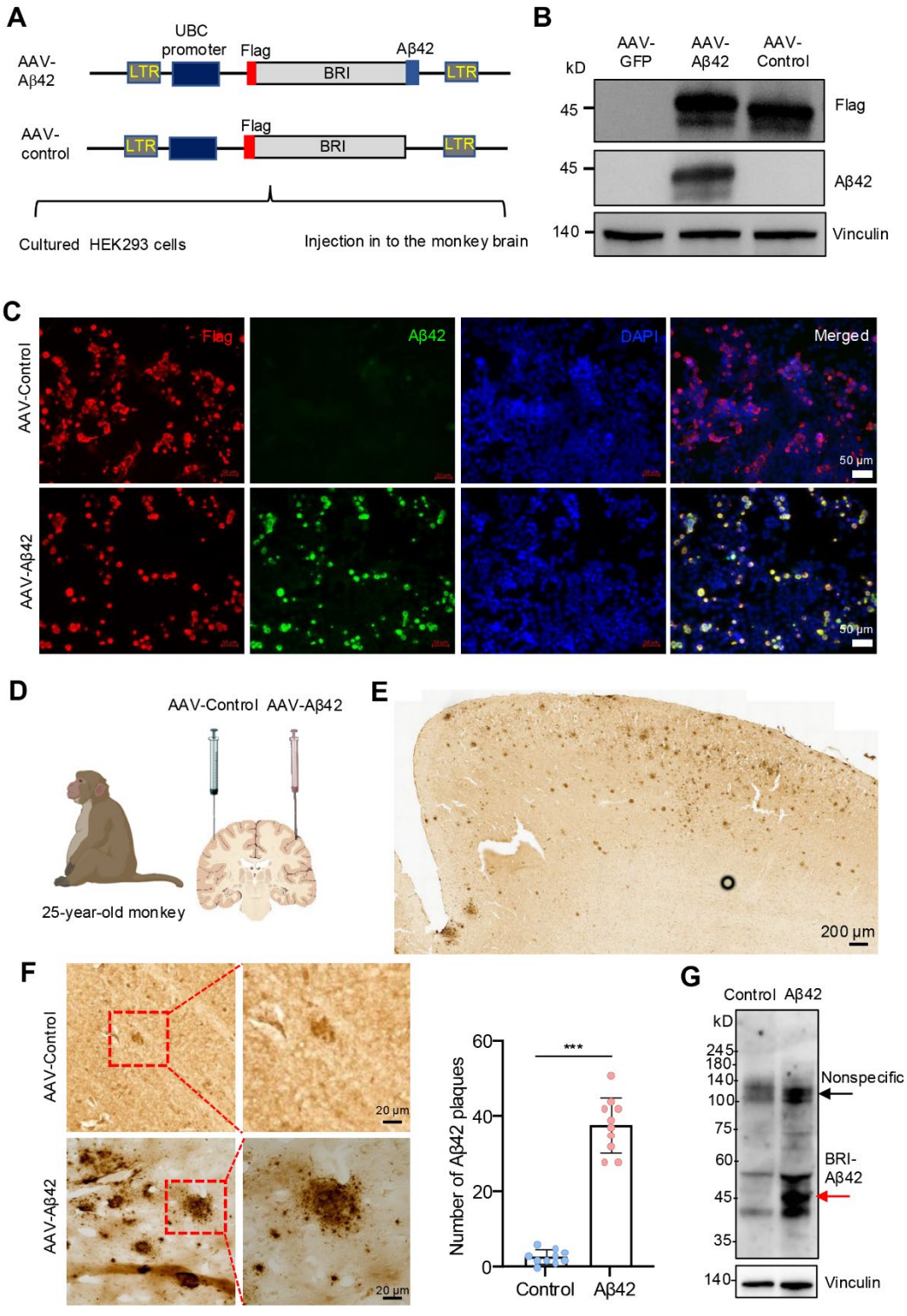

Figure 1. Viral expression of BRI-Aβ42 in the monkey brain

(A) AAV9 vectors for expressing BRI control and BRI-Aβ42. **(B)** Western blotting analysis of HEK293 cells infected by AAV-GFP, AAV-BRI (AAV-Control), and AAV- BRI-Aβ42 (AAV-Aβ42) using anti-flag and anti-Aβ42. **(C)** Immunostaining of transfected HEK293 cells with anti-Aβ42 confirms the expression of Aβ42. **(D)** Brain stereotaxic injection of AAV-Control (10 μL, 1×10^13 vg/mL) and AAV-Aβ42 (10 μL, 1×10^{13} vg/mL) into the prefrontal cortex of an aged monkey (n = 1). **(E, F)** Low **(E)** and high **(F)** magnification micrographs showing that Aβ42 forms significantly more plaques (n = 12 from one animal, *two-tailed student t*-test, *P<0.001*) in the prefrontal cortex injected with AAV-Aβ42 compared to the AAV-BRI injected group. **(G)** Western blotting using anti-Aβ42 verified the expression of Aβ42 in the AAV-Aβ42-injected monkey brain cortex. The data are presented as mean±SEM, ***: *P*<0.001.

Fig. 2

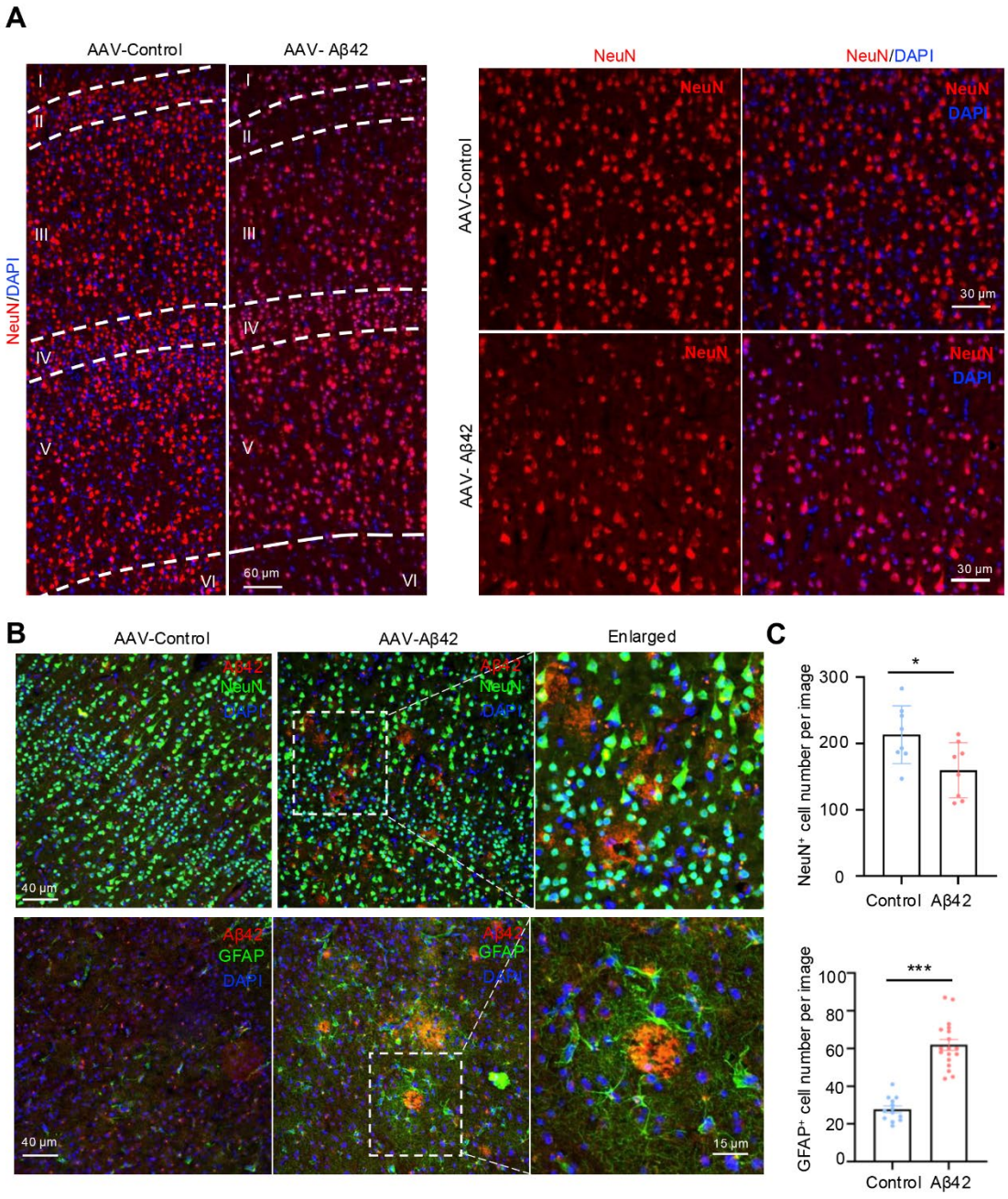

Figure 2. Aβ42 expression in the aged monkey cortex induces neuronal loss

Science Press
ZR Zoological Research

(A) NeuN staining showing the reduced density of NeuN-positive cells in the layer III and layer V regions of AAV-Aβ42-injected (n = 1, 10 μL injected, 1 × 10^13 vg/mL) prefrontal cortex compared to AAV-Control (n = 1, 10 μL injected, 1 × 10^13 vg/mL) of an aged monkey at 25 years of age. The left and right panels show the low and high-magnification micrographs, respectively. **(B)** Double immunostaining of the Aβ42-injected monkey cortex using anti-NeuN or anti-GFAP with anti-Aβ42. **(C)** Quantification of the numbers of NeuN-positive (n⩾8 from one animal, *two-tailed student t*-test, *P<0.05*) and GFAP-positive cells (n⩾12 from one animal, *two-tailed student t*-test, *P<0.001*). The data are presented as mean±SEM, *: *P*<0.05; ***: *P*<0.001.

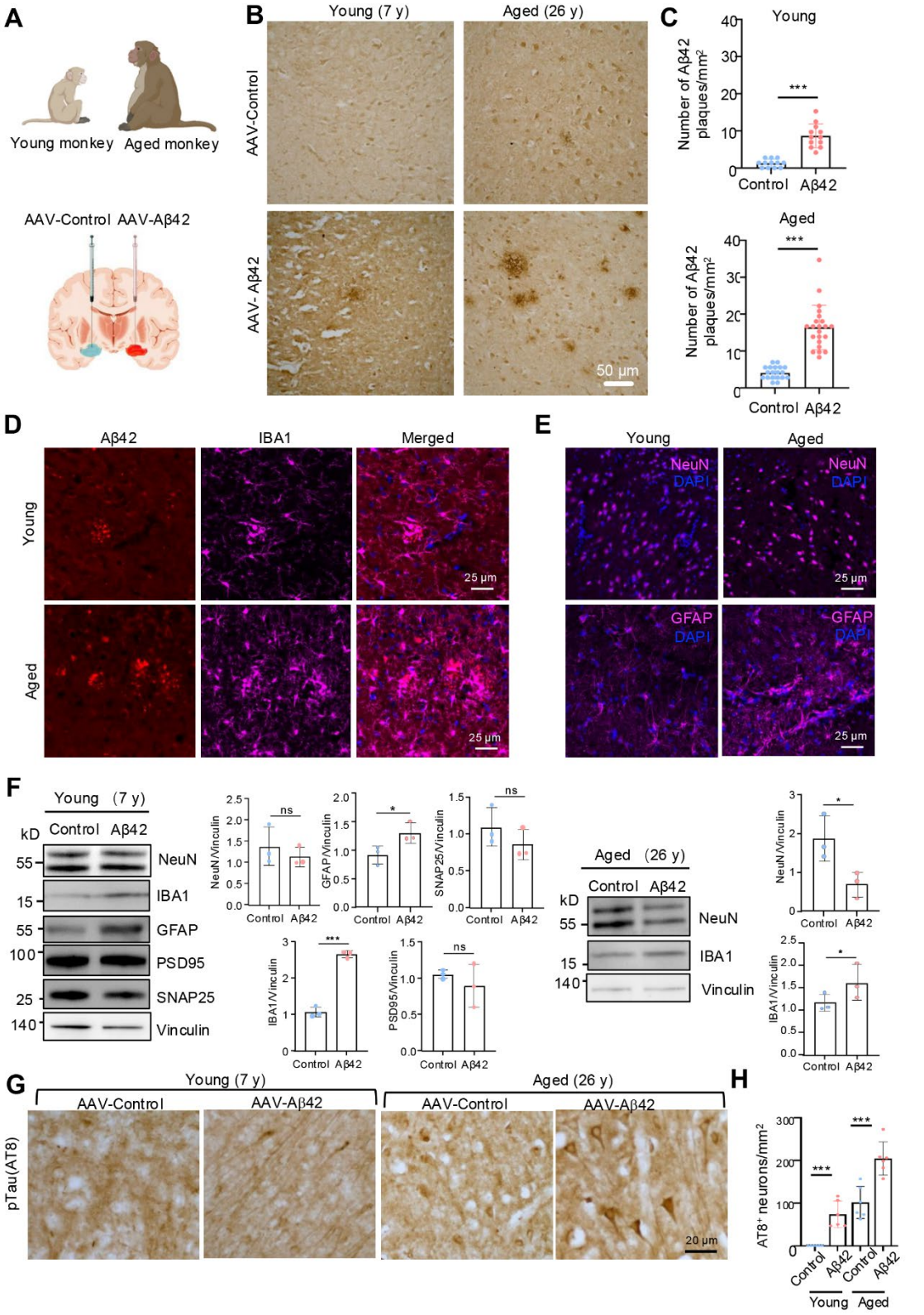

Figure 3. Age-dependent neuropathology of the monkey hippocampus expressing Aβ42

(A) Unilateral injection of AAV-Control or AAV -Aβ42 into the right or left hippocampus of young (~ 7 years) and aged (~ 26 years) monkeys. **(B, C)** Immunostaining (B) and quantification (C) of Aβ42 plaques in the injected monkeys 3 months after injection. (n⩾12 from three animals for the young group, *two-tailed Student's t*-test, *P<0.001*; n⩾24 from three animals for the aged group, *two-tailed Student's t-test*, *P<0.001*) **(D)** Double immunostaining of the Aβ42-injected monkey hippocampus using anti-IBA1 with anti-Aβ42. **(E)** GFAP and NeuN double immunostaining in the young and aged AAV-Aβ42-injected hippocampus. **(F)** Western blotting analysis of neuronal (NeuN, PSD95, synapsin-25) and glial (GFAP and IBA1) proteins in AAV-Control- and AAV-Aβ42-injected hippocampus of young (n = 3 from three animals, *two-tailed student t*-test, NeuN: *P*>0.05; GFAP: *P<0.05*; SNAP25: *P*>0.05; IBA1: *P<0.001*; PSD95: *P*>0.05) and aged monkeys (n=3 from three animals, *two-tailed student t*-test, NeuN: *P<0.05*; IBA1: *P<0.05*). **(G)** Immunostaining with anti-pTau antibody (AT8) showing the increased expression of pTau in the aged hippocampus with AAV-Aβ42 expression. (**H**) Quantification of AT8-positive cells per image (Yong group:n=6 from three animals, *two-tailed student t*-test, *P<0.001*; Aged group:n=6 from three animals, *two-tailed student t*-test, *P<0.001*). The data are presented as mean±SEM, ns: Not significant;*: *P*<0.05; ***: *P*<0.001.

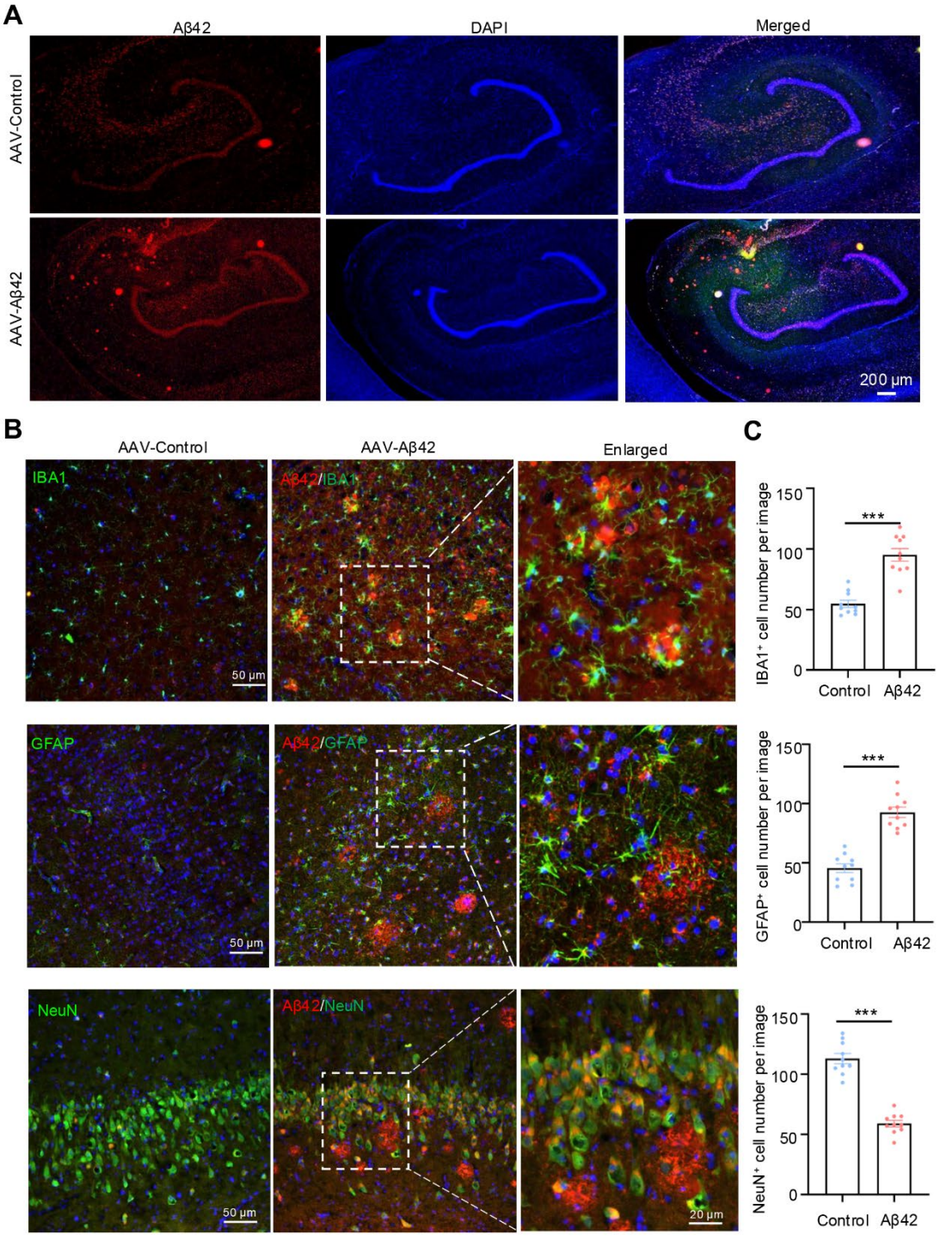

Figure 4. Aβ42-induced neuropathology in the hippocampus of aged monkeys

(A) Aβ42 immunostaining of the hippocampus of an aged monkey at the age of 25 years. **(B)** Immunostaining of the hippocampus of the aged monkey 3 months after AAV-Aβ42 injection. Antibodies to NeuN, GFAP, and IBA1 were used. **(C)** Quantification of the numbers of NeuN, GFAP, or IBA1-positive cells in the control AAV and AAV-BRI-Aβ42 injected hippocampus (n=10 from three animals per group, *two-tailed student t*-test, IBA1: *P<0.001*; GFAP: *P<0.001*; NeuN: *P<0.001*). The data are presented as mean±SEM, ***: *P*<0.001.

Science Press
ZR Zoological Research

Fig. 5

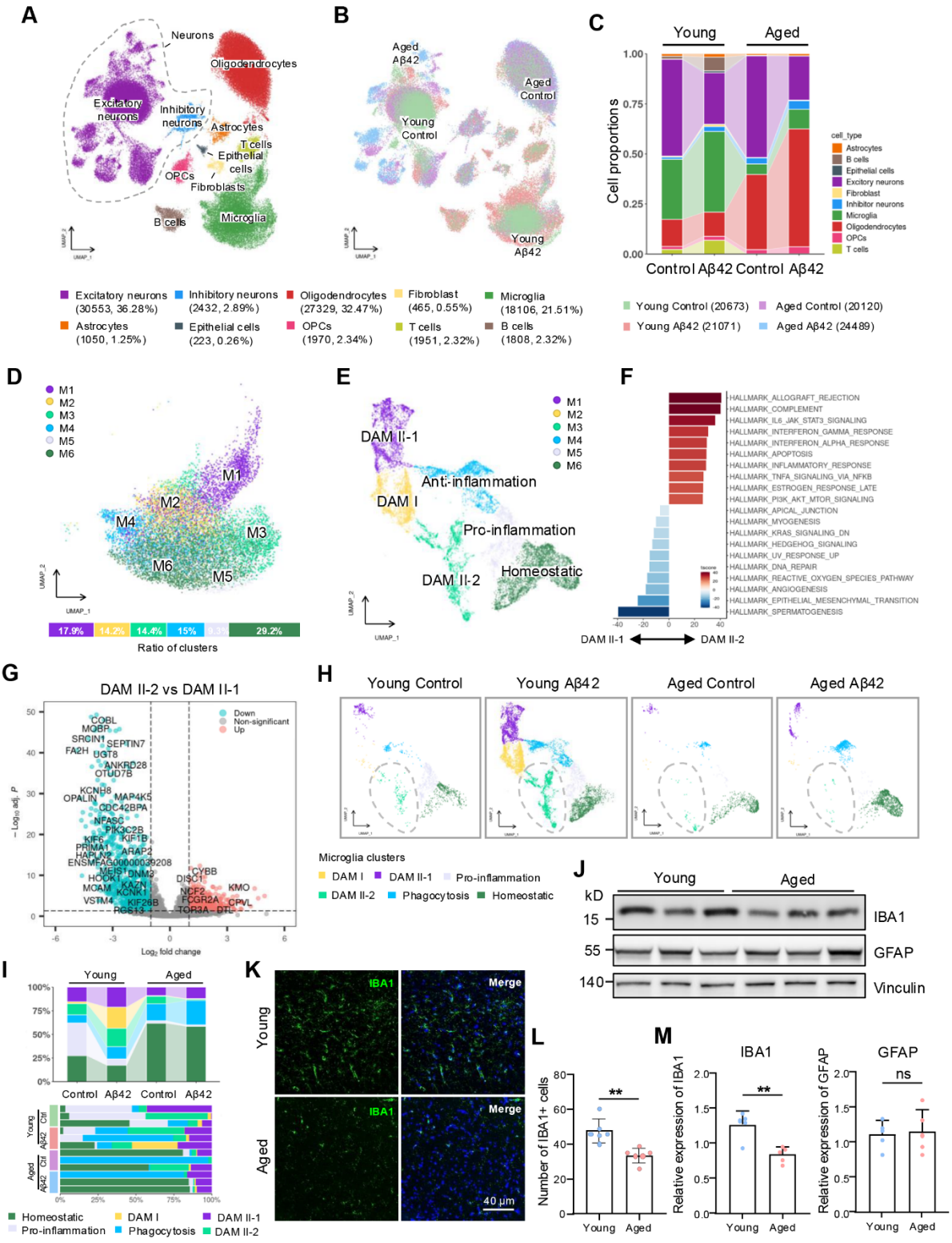

Science Press
ZR Zoological Research

Figure 5. snRNA-seq analysis reveals differences in microglia between young and aged monkey hippocampus

(A-B) UMAP plots showing distinct cell clusters across four groups, with each color representing a unique cell type. **(C)** Bar plot displaying the proportion of each cellular cluster within each group. **(D, E)** The microglia cells were divided into six subclusters according to their biological functions, and the UMAP plot shows the distribution of each subcluster. **(F)** Top enrichment pathways in each subcluster. The red bar represents up-regulated pathways, and the blue represents down-regulated pathways. **(G)** The DEGs between DAM II-2 and DAM II-1 microglia in monkeys. Red dots indicate up-regulated genes, and blue dots indicate down-regulated genes. **(H)** UMAP shows the microglial subclusters in each group, with the dotted line circle highlighting a subcluster that decreases in aged monkeys. **(I)** The proportion of each microglia subcluster within each group and each sample. The DAM II-2 microglia (light green) were decreased in the aged monkey hippocampus. **(J)** The IBA1 immunostaining shows the microglia in the young and aged AAV-Aβ42-injected hippocampus. **(K)** Representative Western blot analysis showing the expression of hippocampal IBA1 and GFAP in 3 young (~11 years) and 3 aged (23-25 years) WT monkeys. **(L)** Quantification of IBA1 positive cells per image in young and aged groups (n=6 from three animals per group, *two-tailed student t*-test, $P<0.01$). **(M)** Quantification of IBA1 and GFAP relative expression levels in the hippocampus of young and aged WT monkeys (n=6 per group, *two-tailed student t*-test, IBA1: $P<0.01$; GFAP: $P>0.05$). The data are presented as mean±SEM, ns: Not significant;*: $P<0.05$; ***: $P<0.001$.

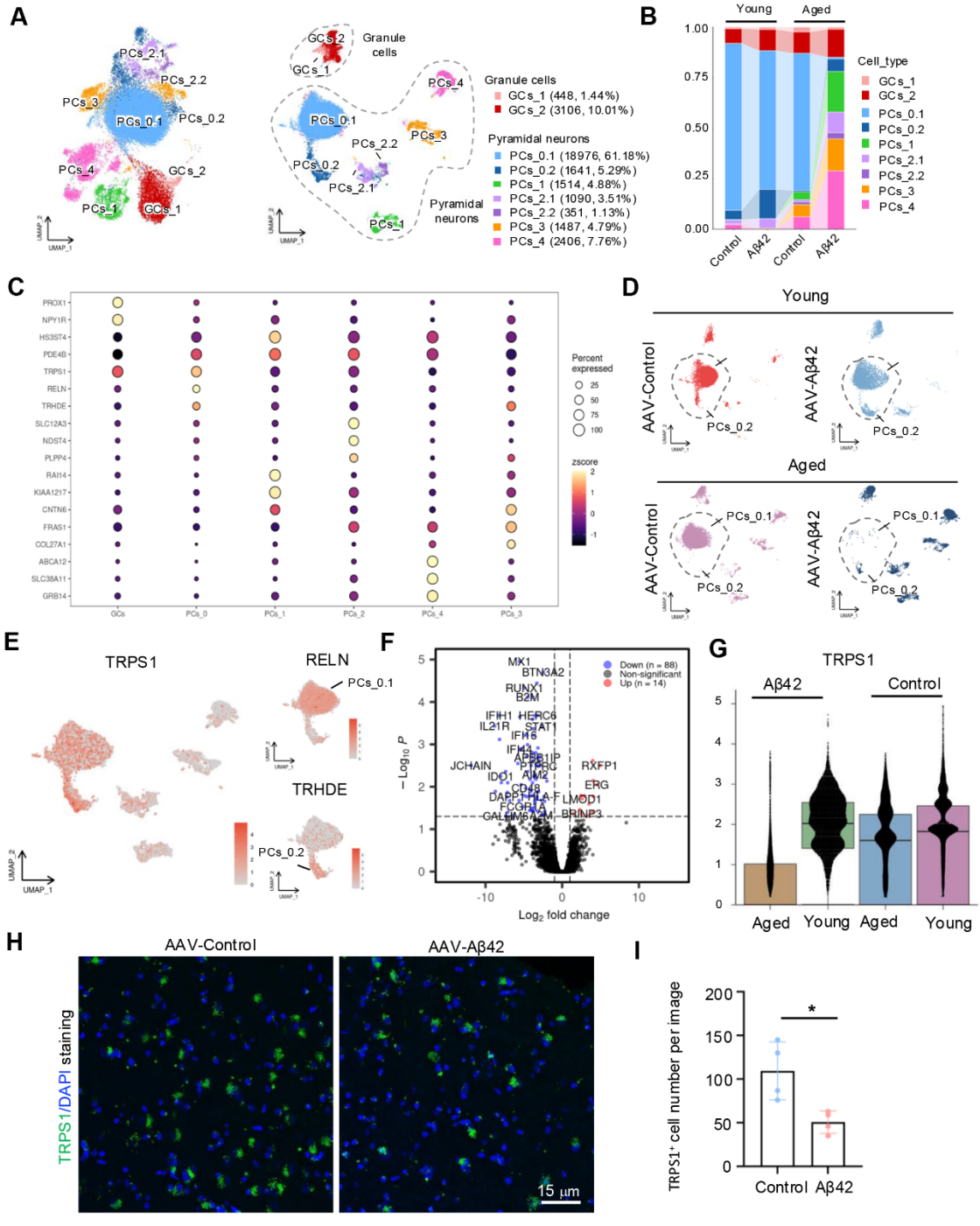

Zoological Research

Figure 6. Aβ42-mediated loss of *TRPS1*$^+$ pyramidal neurons in the aged monkey hippocampus

(A) The UMAP blot of the subclusters of excitatory neurons. The granule cells were subdivided into GCs_0.1 and GCs_2, and the pyramidal neurons were subdivided into PCs_0.1, PCs_0.2, PCs_1, PCs_2.1, PCs_2.2, PCs_3, and PCs_4. Each color represents a unique cell type. **(B)** The cellular proportion of excitatory neuron subclusters in each group. **(C)** The dot plot shows the identified markers for each excitatory subcluster. **(D)** The PCs_0.1 cluster is significantly decreased in the aged Aβ42 group, and the dotted circle highlights PCs_0.1 and PCs_0.2 subclusters. **(E)** The relative expression levels of the marker genes for total PCs_0 (*TRPS1*$^+$), PCs_0.1 (*RELN*$^+$), and PCs_0.2 (*TRHDE*$^+$) in the UMAP. **(F)** The volcano plot shows the DEGs of the PCs_0 clusters between young and aged monkeys injected with AAV-BRI-Aβ42. (**G**) TRPS1 expression was decreased in the aged Aβ42 group. Each dot in the plot indicates one cell in the group. **(H)** Immunofluorescent staining for TRPS1 in the hippocampus shows a reduction of TRPS1 neurons in the aged Aβ42 monkey. (**I**) Quantification of TRPS1$^+$ neurons per image. The average numbers of *TRPS1*$^+$ neurons in different sections of the hippocampus are used for statistical analysis (n=4 from three animals, *two-tailed Student's t*-test). The data are presented as mean±SEM, *: $P<0.05$.

Table 1

Animal No	Sex	Age (year)	Virus	Hippocampal AAV injection	Analyses
Monkey-1	F	23	AAV9-BRI	Bilateral	Behavioral MRI
Monkey-2	F	24	AAV9-BRI	Bilateral	Behavioral MRI
Monkey-3	F	25	AAV9-BRI	Bilateral	Behavioral MRI
Monkey-4	F	25	AAV9-BRI	Bilateral	Behavioral MRI
Monkey-5	F	22	AAV9-BRI-Aβ42	Bilateral	Behavioral MRI
Monkey-6	F	24	AAV9-BRI-Aβ42	Bilateral	Behavioral MRI
Monkey-7	F	23	AAV9-BRI-Aβ42	Bilateral	Behavioral MRI
Monkey-8	F	25	AAV9-BRI-Aβ42	Bilateral	Behavioral MRI
Monkey-9	F	24	AAV9-BRI-Aβ42	Bilateral	Behavioral MRI
Monkey-10	F	25	AAV9-BRI-Aβ42 AAV9-BRI	Left cortex Right cortex	Western blotting
Monkey-11	F	7	AAV9-BRI-Aβ42 AAV9-BRI	Left hippocampus Right hippocampus	Histology snRNAseq
Monkey-12	F	7	AAV9-BRI-Aβ42 AAV9-BRI	Left hippocampus Right hippocampus	Histology snRNAseq
Monkey-13	F	7	AAV9-BRI-Aβ42 AAV9-BRI	Left hippocampus Right hippocampus	Histology snRNAseq

Monkey-14	F	26	AAV9-BRI-Aβ42 AAV9-BRI	Left hippocampus Right hippocampus	Histology snRNAseq
Monkey-15	F	26	AAV9-BRI-Aβ42 AAV9-BRI	Left hippocampus Right hippocampus	Histology snRNAseq
Monkey-16	F	28	AAV9-BRI-Aβ42 AAV9-BRI	Left hippocampus Right hippocampus	Histology snRNAseq

Aβ42 诱导老年食蟹猴海马细胞的选择性丢失

陈来强[1,2#]，张家玮[2#]，王志富[2,3#]，马玉恒[2,3]，林颖琪[2,3]，宋熙辰[2,3]，罗小鹏[2,3]，陈克城[2,3]，王璐[4]，徐浩[4]，李世华[2,3]，闫森[2,3]，王向宇[1]，文军[1*]，杨伟莉[2,3*]，李邦[2,5*]，李晓江[2,3,6*]

1 暨南大学附属第一医院神经外科，广州 510630，中国
2 暨南大学粤港澳中枢神经再生研究院，广东省非人灵长类动物模型研究重点实验室，广州 510632，中国
3 生物活性分子与成药性评估全国重点实验室，广州 510632，中国
4 暨南大学附属第一医院核医学科与 PET/CT-MRI 中心，回旋加速器与 PET 放射性药物中心，广州 510630，中国
5 铜仁学院农林工程与规划学院，贵州 铜仁 554300，中国
6 临港实验室，上海 201306，中国

前三位作者对本研究贡献相同（共同第一作者）
* 后四位作者对本研究贡献相同（共同通讯作者）

主要联系人: 李晓江
邮箱: xjli33@jnu.edu.cn,
暨南大学粤港澳中枢神经再生研究院, 广州 510632，中国

摘要： 海马是阿尔茨海默病（AD）中最早受累且受损最严重的脑区之一，其对记忆的形成至关重要。然而，AD 疾病中海马神经元丢失的确切机制目前还尚不十分明确。为了在与人类更接近的动物模型中探索 Aβ42 的毒性作用，我们将编码人 Aβ42 的 AAV9 病毒载体立体定向注射到青年（7 岁）和老年（>20 岁）食蟹猴的海马脑区中。研究发现，与青年对照组相比，AAV9 介导的 Aβ42 过表达在老年猴海马脑区中诱发了更为严重的神经病理学改变，导致其日间活动减少且睡眠障碍加剧。单核 RNA 测序（snRNA-seq）结果显示，老年猴海马中疾病相关小胶质细胞（DAM II）呈现年龄依赖性的减少。此外，我们鉴定出一类特定亚型的海马锥体神经元（*TRPS1*$^{+}$*RELN*$^{+}$），该类神经元在老年猴中对 Aβ42 毒性表现出选择性丢失。本研究结果表明，小胶质细胞的衰退与特定神经元亚型（*TRPS1*$^{+}$*RELN*$^{+}$锥体细胞）的选择性丢失共同作用，加剧了 Aβ42 在老年灵长类动物海马脑区中的毒性。本研究所新鉴定出的这一神经元亚型，有望成为治疗 AD 疾病海马损伤的潜在全新靶点。

关键词： 阿尔茨海默病；淀粉样蛋白病理；非人灵长类动物；衰老；神经退行性变